

Preference-Aligned LoRA Merging: Preserving Subspace Coverage and Addressing Directional Anisotropy

Wooseong Jeong*
KAIST

stk14570@kaist.ac.kr

Wonyoung Lee*
KAIST

wylee@kaist.ac.kr

Kuk-Jin Yoon
KAIST

kjyoon@kaist.ac.kr

Abstract

Merging multiple Low-Rank Adaptation (LoRA) modules is promising for constructing general-purpose systems, yet challenging because LoRA update directions span different subspaces and contribute unevenly. When merged naively, such mismatches can weaken the directions most critical to certain task losses while overemphasizing relatively less important ones, ultimately reducing the model’s ability to represent all tasks faithfully. We revisit this problem through two perspectives: *subspace coverage*, which captures how broadly LoRA directions cover diverse representational directions, and *anisotropy*, which reflects the imbalance of influence across those directions. We propose TARA-Merging (Task-Rank Anisotropy Alignment), which aligns merging weights using a preference-weighted cross-entropy pseudo-loss while preserving task-relevant LoRA subspaces. This ensures broad subspace coverage and mitigates anisotropy via direction-wise reweighting. Across eight vision and six NLI benchmarks, TARA-Merging consistently outperforms vanilla and LoRA-aware baselines, demonstrating strong robustness and generalization, and highlighting the importance of addressing both subspace coverage and anisotropy in LoRA merging. Code is available at <https://github.com/wooseong97/TARA-Merge>.

1. Introduction

Low-Rank Adaptation (LoRA) [29] is widely used to adapt large foundation models to downstream tasks, including large language models and vision-language models such as CLIP [72]. By introducing lightweight low-rank adapters, LoRA enables efficient fine-tuning with far fewer trainable parameters and reduced memory overhead, while mitigating the risk of overfitting when only limited data are available. This efficiency has encouraged training separate LoRA adapters on many different datasets, each capturing distinct aspects of vision or language understanding. Com-

binning task-specific LoRA modules into a single network falls under the paradigm of *model merging* [102], which provides an attractive alternative to costly multi-task training [35–38] and enables the construction of general-purpose models that flexibly integrate knowledge across tasks and reflect different task preferences.

Recent research has explored various model merging. Early baselines such as task arithmetic [32, 39, 68] treat fine-tuned models as linear updates and combine them through a linear combination. Ties-merging [99] and DARE [107] reduces interference by dropping parameters, while AdaMerging [101] adapts merging coefficients using gradients derived from an entropy-based surrogate loss. Recent work has targeted model merging specifically for LoRA. KnOTS [79] aligns adapters using a shared SVD basis, and LoRA-LEGO [114] clusters rank-wise units to preserve modularity. Focusing on LoRA adapters is promising, as LoRA fine-tuning has become standard practice for modern LLMs and VLMs. Moreover, operating at the adapter level substantially reduces memory and compute overhead compared to merging full model weights, enabling even gradient-based approaches such as AdaMerging to scale to foundation models. In addition, While several approaches have been proposed, they often overlook at least one of the two fundamental challenges we emphasize in this work, namely preserving subspace coverage and addressing directional anisotropy.

LoRA produces a low-rank update that we decompose into rank-wise components for analysis. We collectively term these directions as *LoRA directions*. With this setup, two aspects are essential for successful merging: *subspace coverage* and *anisotropy*. Subspace coverage captures how widely the LoRA directions collectively span the representational subspace, so preserving coverage ensures access to diverse task-relevant information. Anisotropy refers to directional sensitivity imbalance. Even with sufficient coverage, task losses can be unequally sensitive to different LoRA directions, which can distort trade-offs if ignored. Furthermore, when task preferences are specified, effective merging must preserve coverage while aligning merg-

*Equal contribution to this work.

ing weights with those preferences. Most merging methods address only one side of the problem. Task arithmetic and pruning reduce interference but erode subspace coverage and ignore direction-wise sensitivity. AdaMerging tunes global weights yet misses per-direction anisotropy. LoRA-aware methods like KnOTS and LoRA-LEGO improve structure but can shrink effective coverage and still lack sensitivity weighting. In short, they do not jointly preserve coverage and model anisotropy over LoRA directions.

Building on these observations, we propose TARA, short for *Task-Rank Anisotropy Alignment*. Our method introduces a structured merging framework that explicitly incorporates task preferences while addressing the two properties above. It preserves LoRA directions to maintain subspace coverage and accounts for anisotropy by direction-wise reweighting according to sensitivity. It then aligns the merging weights with a preference-weighted entropy pseudo loss, yielding merged models that faithfully approximate fine-tuned models across tasks while improving robustness and generalization. We validate our approach across eight vision datasets and six natural language inference tasks, where TARA consistently outperforms vanilla baselines and recent LoRA-aware methods in joint-task evaluation and transfer to unseen tasks.

Our main contributions are summarized as follows:

- Identification of **subspace coverage** and **anisotropy** as two key properties for analyzing and guiding LoRA merging, highlighting their roles in subspace preservation and direction-wise sensitivity.
- Introduction of **TARA**, a framework that aligns both task-level and rank-level preferences, ensuring coverage of LoRA subspaces while mitigating anisotropy-induced imbalance.
- Extensive empirical validation on vision and language benchmarks, demonstrating state-of-the-art performance and strong robustness in various experimental settings.

2. Related work

Model Merging. Model merging integrates knowledge from separately fine-tuned models without joint multi-task training [], reducing computational cost while preserving task performance [23, 60, 102]. Core baselines include *Task Arithmetic*, which adds or subtracts task vectors [32], *Reg-Mean*, which requires inner-product matrices of layer inputs for data-free fusion [40], *TIES*, which resolves sign conflicts and prunes small deltas [99], and *DARE*, which sparsifies update deltas [107]. *AdaMerging* learns layer-wise merge coefficients via entropy minimization to improve multi-task performance [101]. For models trained on different data or from different initializations, permutation alignment preserves linear mode connectivity [1, 21]. *ZipIt* matches intermediate features to re-basin networks and align neu-

rons across models, enabling training-free layer alignment [78]. Uncertainty-aware combinations mitigate mismatch through Fisher-weighted averaging [63] and uncertainty or gradient matching [13]. Preference-aware settings motivate multi-objective formulations such as Pareto merging [7] and smooth scalarization [49]. Overall, recent work advances simple averaging into alignment- and uncertainty-aware schemes with explicit trade-off control.

LoRA-aware Merging. For large networks including foundation models such as LLMs [19], Low-Rank Adaptation (LoRA) [29] is a widely used fine-tuning scheme. Conventional parameter-space merging methods [32, 40, 99, 107] transfer poorly to LoRA adapters, motivating LoRA-aware approaches [79, 84, 114]. In particular, Stoica et al. [79] argue that LoRA-updated models exhibit weaker cross-model representation alignment than full-rank finetunes, and propose KNOTS, which concatenates adapter updates and applies an SVD to align them in a shared subspace before merging principal components. Zhao et al. [114] introduce *minimal semantic units* (MSUs) and perform clustering to assemble a merged adapter with an adjustable effective rank. Related mixtures of LoRAs have also been explored for image generation, including multi-LoRA composition and concept mixing [22, 117, 120]. Additional related work and connections to our approach are discussed in Section B.

General model merging ignore the factorized structure of LoRA and often suffer from strong misalignment when adapters are folded into the base model before merging. In contrast, LoRA-aware methods operate on the low-rank factors, which is both efficient and more effective for combining updates. In this work we explicitly account for *subspace coverage* and *anisotropy*, two critical aspects of LoRA merging that prior methods largely overlook.

3. Subspace Coverage and Anisotropy

3.1. Problem Setting and Notation

Modern foundation models in language and vision are increasingly adapted with LoRA rather than full fine-tuning, which motivates principled ways to combine many LoRA adapters into a single model. In practice, directly merging adapters by folding them into the base weights and applying model-merging often underperforms due to strong cross-task misalignment [79]. These factors call for a merging approaches that is aware of the LoRA structure. We therefore study *LoRA merging*, where multiple LoRA fine-tuned adapters are combined into one model that balances task performance according to a user-specified preference.

Base model and LoRA adapters. Let $W_0 \in \mathbb{R}^{d \times m}$ be the frozen pretrained weight matrix. For each task $i \in \{1, \dots, N\}$, we attach a LoRA adapter of rank r_i , parame-

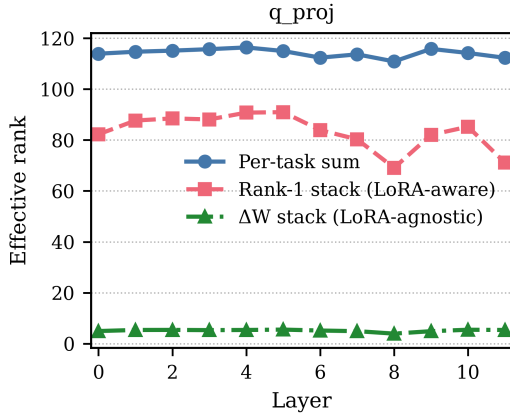


Figure 1. **Effective rank** across layers for an attention projection layer (e.g., query). The gap between ΔX stack and Rank-1 stack reflects merge-induced collapse.

terized as

$$\Delta W_i = B_i A_i^\top, \quad B_i \in \mathbb{R}^{d \times r_i}, \quad A_i \in \mathbb{R}^{m \times r_i}. \quad (1)$$

Thus, $\text{rank}(\Delta W_i) \leq r_i \ll \min(d, m)$. We further decompose each as $\Delta W_i = \sum_{j=1}^{r_i} \mathbf{b}_{ij} \mathbf{a}_{ij}^\top$, where \mathbf{b}_{ij} and \mathbf{a}_{ij} denote the j -th columns of B_i and A_i . Each outer product $\mathbf{b}_{ij} \mathbf{a}_{ij}^\top$ is referred to as a *rank-1 LoRA direction*.

User preferences. We assume that the relative importance of tasks is specified by a vector $\boldsymbol{\rho} = [\rho_1, \dots, \rho_N]^\top \in \Delta_{N-1}$, where Δ_{N-1} denotes the probability simplex. A larger ρ_i indicates higher priority for task i .

Merging as Multi-Objective Optimization. Without fixing preferences, LoRA merging can be cast as a multi-objective optimization (MOO) problem [65] that seeks a set of solutions. We minimize the objective vector $\mathbf{f}(\mathbf{W}) = [f_1(\mathbf{W}), \dots, f_N(\mathbf{W})]^\top$ over merged models \mathbf{W} obtained by linearly combining available LoRA adapters on top of a fixed base \mathbf{W}_0 . A solution \mathbf{W}^a *dominates* \mathbf{W}^b if $f_k(\mathbf{W}^a) \leq f_k(\mathbf{W}^b)$ for all $k \in \{1, \dots, N\}$ and $f_j(\mathbf{W}^a) < f_j(\mathbf{W}^b)$ for some j . A solution is *Pareto optimal* if no other feasible solution dominates it. The *Pareto front* is the collection of Pareto-optimal solutions.

3.2. Preserving LoRA Subspace Coverage

We quantify how much task-specific representational capacity is retained when LoRA adapters are merged. We refer to this as *subspace coverage*: it measures how broadly the task-specific LoRA directions span the parameter space and how well a merge preserves that span. We measure subspace coverage using the entropy-based *effective rank* (erank) [73]. Let $\mathbf{X} \in \mathbb{R}^{d \times m}$ have singular values $\{\sigma_k\}_{k=1}^{r_X}$ where $r_X = \text{rank}(\mathbf{X})$, and define $p_k = \sigma_k^2 / \sum_{j=1}^{r_X} \sigma_j^2$.

Then the effective rank is

$$\text{erank}(\mathbf{X}) = \exp\left(-\sum_{k=1}^{r_X} p_k \log p_k\right). \quad (2)$$

$\text{erank}(\mathbf{X})$ equals r_X for a flat spectrum and decreases as energy concentrates, providing a basis-invariant measure of effective dimensionality.

We compare three quantities using effective rank, with all stacks formed by vectorizing matrices and placing one vector per row. First, *per-task sum* computes erank for each task i on $\mathbf{X}_i = [\text{vec}(\mathbf{b}_{i1} \mathbf{a}_{i1}^\top), \dots, \text{vec}(\mathbf{b}_{ir_i} \mathbf{a}_{ir_i}^\top)]^\top$ and then sums $\sum_{i=1}^N \text{erank}(\mathbf{X}_i)$. Second, the ΔX stack (*LoRA-agnostic*) uses $\mathbf{X}_{\text{agnostic}} = [\text{vec}(\Delta \mathbf{W}_1), \dots, \text{vec}(\Delta \mathbf{W}_N)]^\top$ and computes a single $\text{erank}(\mathbf{X}_{\text{agnostic}})$. Third, the Rank-1 stack (*LoRA-aware*) aggregates all rank-1 factors across tasks into $\mathbf{X}_{\text{aware}} = [\text{vec}(\mathbf{b}_{11} \mathbf{a}_{11}^\top), \dots, \text{vec}(\mathbf{b}_{Nr_N} \mathbf{a}_{Nr_N}^\top)]^\top$ and computes $\text{erank}(\mathbf{X}_{\text{aware}})$. Here we refer to the Rank-1 stack as *LoRA-aware* because it preserves the adapter factorization and treats each rank-1 direction $\mathbf{b}_{ij} \mathbf{a}_{ij}^\top$ as a separate basis element, whereas the ΔW stack is *LoRA-agnostic* since it collapses each adapter into a single update $\Delta \mathbf{W}_i$ and ignores the internal rank-1 structure.

As shown in Figure 1, the *LoRA-aware* stack retains about 70% of the *per-task sum*, indicating that most task-specific directions remain approximately independent after redundancy removal and thus cross-task alignment is weak. This agrees with prior work showing that LoRA fine-tuned models align less across tasks than full-rank fine-tuning [79]. The gap between the *LoRA-aware* and *LoRA-agnostic* stacks captures subspace collapse under interpolation-based merging [32, 99, 101], because unlike $\mathbf{X}_{\text{aware}}$ the interpolated updates in $\mathbf{X}_{\text{agnostic}}$ can interfere destructively across tasks and lower the effective rank. Formal definitions and additional results appear in Section D of supplementary material.

3.3. Anisotropy of LoRA Directions

Let \mathbf{W} be the current weights and $\{\mathbf{S}_k\}_{k=1}^K$ a set of *LoRA directions*, where a LoRA adapter uses factor matrices $\mathbf{B} \in \mathbb{R}^{d \times r}$ and $\mathbf{A} \in \mathbb{R}^{m \times r}$ (for simplicity, the same rank r for all adapters), with columns \mathbf{b}_k and \mathbf{a}_k , and we set $\mathbf{S}_k = \mathbf{b}_k \mathbf{a}_k^\top$ (so $K = r$ for a single adapter, or the sum of ranks if multiple adapters are stacked). Consider a small update restricted to this span with *direction-selection coefficients* $\boldsymbol{\phi} = (\phi_1, \dots, \phi_K)^\top \in \mathbb{R}^K$ (distinct from the task-preference vector $\boldsymbol{\rho}$), so that $\Delta \mathbf{W} = \sum_{k=1}^K \phi_k \mathbf{S}_k$. Using the Frobenius inner product, the first-order change of each task loss is

$$\Delta f_i \approx \langle \nabla f_i(\mathbf{W}), \Delta \mathbf{W} \rangle_F = \sum_{k=1}^K \phi_k \langle \nabla f_i(\mathbf{W}), \mathbf{S}_k \rangle_F. \quad (3)$$

Stacking $\Delta \mathbf{f} = [\Delta f_1, \dots, \Delta f_N]^\top$ yields the linearization

$$\Delta \mathbf{f} \approx \mathbf{J} \phi, \quad \mathbf{J}_{i,k} = \langle \nabla f_i(\mathbf{W}), \mathbf{S}_k \rangle_F, \quad (4)$$

so $\mathbf{J}(\mathbf{W})$ is the task-loss Jacobian restricted to $\text{span}\{\mathbf{S}_k\}$. Directional imbalance is captured by the singular values of \mathbf{J} , which give the following bound from coefficients to loss changes.

Proposition 1 (Anisotropy Bounds). *Let $\sigma_{\max}(\mathbf{J})$ and $\sigma_{\min}(\mathbf{J})$ denote the largest and smallest singular values of \mathbf{J} . Then, for any coefficient vector ϕ ,*

$$\sigma_{\min}(\mathbf{J}) \|\phi\|_2 \leq \|\mathbf{J}\phi\|_2 = \|\Delta \mathbf{f}\|_2 \leq \sigma_{\max}(\mathbf{J}) \|\phi\|_2. \quad (5)$$

When $\kappa(\mathbf{J}) = \sigma_{\max}(\mathbf{J})/\sigma_{\min}(\mathbf{J})$ is large, the map $\phi \mapsto \Delta \mathbf{f}$ is anisotropic, and equal-norm LoRA-direction updates need not yield proportional task-loss changes.

Empirical evidence of anisotropy. To illustrate the qualitative effect anticipated by Proposition 1, we measure singular-value spectra and condition numbers of \mathbf{J} across layers and modules. We observe a pronounced spectral spread and large condition numbers, indicating that a few directions dominate the task-loss response while many are weak. Full plots are deferred to Sec. E of supplementary material. See the condition-number traces in Figs. 6 and 7 and the scree curves in Fig. 8 of supplementary material.

Directional-sensitivity misalignment across preferences.

With the scalarized gradient $g(\rho; \mathbf{W}) = \sum_i \rho_i \nabla f_i(\mathbf{W})$, define direction-wise *loss sensitivities*

$$h_k(\rho; \mathbf{W}) = \langle g(\rho; \mathbf{W}), \mathbf{S}_k \rangle_F, \quad (6)$$

$$\mathbf{h}(\rho; \mathbf{W}) = (h_1, \dots, h_K)^\top. \quad (7)$$

When the preference ρ changes, the pattern of $\mathbf{h}(\rho; \mathbf{W})$ also changes as well. We quantify *Directional Sensitivity Misalignment* by

$$\xi(\rho_1, \rho_2; \mathbf{W}) = 1 - \frac{|\langle \mathbf{h}(\rho_1; \mathbf{W}), \mathbf{h}(\rho_2; \mathbf{W}) \rangle|}{\|\mathbf{h}(\rho_1; \mathbf{W})\|_2 \|\mathbf{h}(\rho_2; \mathbf{W})\|_2}, \quad (8)$$

so that $\xi \in [0, 1]$. Here $\langle \cdot, \cdot \rangle$ denotes the dot product. Smaller ξ indicates weaker ρ -dependence of the sensitivity profiles, whereas larger ξ indicates stronger ρ -dependence. When measuring anisotropy, a 180° flip lies in the same one-dimensional span. We therefore treat sign flips as equivalent and focus on alignment along the direction axis.

We quantify how loss-sensitive directions within the LoRA span change when the task preference switches from ρ_1 (uniform over tasks) to ρ_2 (one-hot on a single task). For each preference, we form a sensitivity profile over LoRA directions by projecting the scalarized gradient $g(\rho; \mathbf{W}) = \sum_i \rho_i \nabla f_i(\mathbf{X})$ onto the basis $\{\mathbf{S}_k\}$. Throughout this analysis, we set \mathbf{W} to the Task Arithmetic merge $\mathbf{W}_{\text{merge}} =$

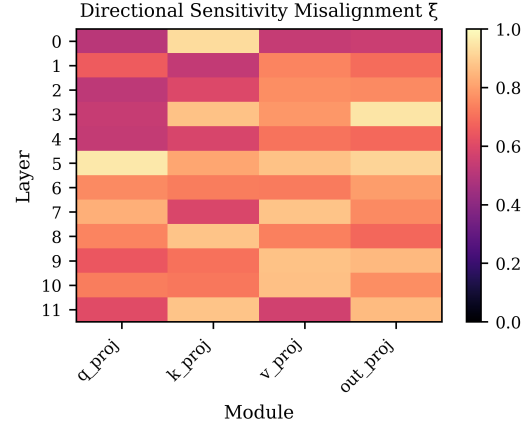


Figure 2. **Directional-sensitivity misalignment** $\xi(\rho_1, \rho_2)$. Larger ξ indicates stronger change in loss-sensitive directions when switching preferences.

$\mathbf{W}_0 + \lambda \sum_{i=1}^N \Delta \mathbf{W}_i$ with $\lambda = 0.3$ following [32]. We then summarize the distance between the two preference with a misalignment index $\xi(\rho_1, \rho_2) \in [0, 1]$. Figure 2 shows substantial misalignment across layers and modules, indicating that directional sensitivities within the LoRA span are highly preference-dependent and motivating our subsequent directional alignment.

4. Method

Based on the analysis, we propose TARA, *Task-Rank Anisotropy Alignment*, which addresses both *subspace coverage* and *anisotropy* in LoRA merging. TARA weights LoRA directions with an entropy-minimization term, as in AdaMerging [101]. We present two variants that specify how the directions are constructed and how the direction-selection weights are assigned.

Variant A: Per-rank LoRA direction selection. This variant reweights individual rank-1 factors and focuses on anisotropy control within each adapter. Let $\phi_{ij} \in \mathbb{R}$ be a *direction-selection weight* for factor (i, j) with $i \in \{1, \dots, N\}$ and $j \in \{1, \dots, r_i\}$. The merged weight is

$$\mathbf{W}_A(\phi) = \mathbf{W}_0 + \sum_{i=1}^N \sum_{j=1}^{r_i} \phi_{ij} \mathbf{b}_{ij} \mathbf{a}_{ij}^\top. \quad (9)$$

Unless otherwise noted, we allow signed weights and learn their scale directly.

Variant B: Shared singular-direction selection. This variant builds a shared orthonormal basis across tasks to preserve subspace coverage, reduce cross-task interference, and control anisotropy via weights. Form a matrix by *horizontally* concatenating adapters as follows:

$$\mathbf{X} = [\Delta \mathbf{W}_1, \dots, \Delta \mathbf{W}_N] \in \mathbb{R}^{d \times (mN)}, \quad (10)$$

Table 1. Per-task accuracy on eight image-classification benchmarks. We merge eight ViT-B/32 checkpoints, each fine-tuned with LoRA. The upper panel shows the per-task absolute accuracy of the fine-tuned baselines. The lower panel shows the accuracy of the merged models, normalized by their corresponding fine-tuned baseline (%).

Method	Dataset								
	Cars	DTD	EuroSAT	GTSRB	MNIST	RESISC45	SUN397	SVHN	Avg
<i>Per-task absolute accuracies (%)</i>									
Finetuned	74.0	58.3	99.0	92.7	99.3	88.4	64.5	96.2	84.1
<i>Per-task accuracies of merged models, normalized to finetuned (%)</i>									
Vanilla Merging									
RegMean [40]	80.2	71.3	37.9	47.3	43.1	70.5	93.9	43.0	60.9
TA [32]	82.1	74.3	48.7	41.8	53.4	71.5	96.6	42.0	63.8
TIES [99]	81.0	72.5	53.8	37.4	69.0	65.3	94.8	45.3	64.9
DARE-TIES [107]	81.6	74.5	51.0	37.2	59.2	66.6	96.0	38.8	63.1
EMR-Merging [31]	82.6	73.9	48.2	40.2	54.6	70.6	95.7	45.9	64.0
FR-Merging [115]	79.9	71.0	24.2	34.2	46.6	65.4	92.2	47.6	57.6
Iso-C [60]	82.0	82.1	55.2	73.0	68.9	80.3	97.7	49.6	73.6
Iso-CTS [60]	80.8	82.3	56.2	74.8	68.5	79.6	97.4	48.5	73.5
AdaMerging [101]	79.5	73.5	70.9	39.7	63.0	69.0	97.8	66.6	70.0
LoRA-aware Merging									
SVD [84]	81.8	73.5	47.7	38.3	52.8	70.2	96.4	40.4	62.6
Linear [59]	81.4	74.5	49.5	43.0	55.3	70.3	96.8	39.0	63.7
KnOTS-TIES [79]	82.7	73.7	49.3	48.9	68.9	70.9	95.5	53.8	68.0
KnOTS-DARE-TIES [79]	81.8	75.9	50.7	40.3	53.2	70.2	97.9	41.0	63.9
LoRA-LEGO [114]	81.1	73.0	54.4	40.3	48.6	71.5	97.3	37.1	62.9
RobustMerge [109]	80.1	76.8	54.8	38.2	55.4	69.5	96.5	35.2	63.3
TARA-Variant A	82.2	76.0	74.9	43.5	76.3	70.2	98.0	70.8	74.0
TARA-Variant B	86.2	78.4	76.8	42.9	82.7	75.4	98.6	69.7	76.3

and compute the SVD: $\mathbf{X} = \mathbf{U}\mathbf{\Sigma}\mathbf{V}^\top$. Select the top R singular values and their associated singular vectors, yielding

$$\mathbf{U} = [\mathbf{u}_1, \dots, \mathbf{u}_R] \in \mathbb{R}^{d \times R}, \quad (11)$$

$$\mathbf{\Sigma} = \text{diag}(\sigma_1, \dots, \sigma_R), \quad (12)$$

$$\mathbf{V} = [\mathbf{v}_1, \dots, \mathbf{v}_R] \in \mathbb{R}^{(mN) \times R}. \quad (13)$$

Partition each \mathbf{v}_k into $\mathbf{v}_k = [\mathbf{v}_{k1}^\top, \dots, \mathbf{v}_{kN}^\top]^\top$ with each $\mathbf{v}_{ki} \in \mathbb{R}^m$ and define

$$\mathbf{S}_{ik} = \mathbf{u}_k \mathbf{v}_{ki}^\top \in \mathbb{R}^{d \times m} \quad (14)$$

Assign weights $\phi_{ik} \in \mathbb{R}$ to these directions and obtain

$$\mathbf{W}_B(\phi) = \mathbf{W}_0 + \sum_{i=1}^N \sum_{k=1}^R \phi_{ik} \sigma_k \mathbf{u}_k \mathbf{v}_{ki}^\top. \quad (15)$$

Together, the shared orthonormal left directions $\{\mathbf{u}_k\}_{k=1}^R$ and the per-task partitions of the right singular vectors preserve subspace coverage. The left basis $\{\mathbf{u}_k\}$ retains the top- R column space of \mathbf{X} , and $\mathbf{v}_{ki} \in \mathbb{R}^m$ yields *rank-1 components* $\mathbf{S}_{ik} = \mathbf{u}_k \mathbf{v}_{ki}^\top$. Direction weights then adjust these rank-1 components preserving subspace coverage.

Variant B incurs extra cost to compute the shared SVD basis, whereas Variant A avoids this step. In return Variant B typically attains higher accuracy, reflecting a practical trade-off between compute and performance. We quantify this trade-off in Table 6 of the supplementary material.

Following Lin et al. [49], we optimize ϕ under a preference vector ρ . Let $\mathbf{W}(\phi)$ denote either $\mathbf{W}_A(\phi)$ from Eq. (9) or $\mathbf{W}_B(\phi)$ from Eq. (15).

Smooth Tchebycheff Scalarization. With anchors $z_i = \min_{\mathbf{W}} f_i(\mathbf{W})$, define

$$\Psi(\phi, \rho) = \alpha \log \left(\sum_{i=1}^N \exp \left(\frac{\rho_i |f_i(\mathbf{W}(\phi)) - z_i|}{\alpha} \right) \right), \quad (16)$$

Here z_i acts as a task-wise anchor that normalizes scale differences across tasks. The parameter $\alpha > 0$ controls smoothing: *smaller* α concentrates the objective on the worst-performing task, whereas *larger* α yields a smoother aggregation that spreads focus more evenly across tasks. During merging, we use predictive entropy following AdaMerging [101] since f_i requires labels. For z_i , we use the entropy loss obtained when only task i 's adapter is applied.

Earlier learning-free mergers were attractive for full-parameter models due to lower memory use and simplicity. In LoRA-adapted settings, however, the memory gap between learning-free and learning-based approaches is small even at foundation-model scale, so there is less reason to insist on learning-free methods. We quantify this in Table 6 of the supplementary material.

5. Experiments

Experimental Setup.

For vision experiments, we follow Stoica et al. [79] and use CLIP [72] with a ViT-B/32 backbone [17] pre-trained on ImageNet-21k [16]. Models are fine-tuned with rank-16 LoRA unless noted otherwise and evaluated on eight image classification benchmarks. We also test our method on six classification datasets with the LLaMA-3 8B model [19].

Dataset descriptions are in Section C.1, and LoRA fine-tuning details in Section C.2 of supplementary material.

Baselines. We denote the pretrained weights by \mathbf{W}_0 , the task vector of the i -th task by $\Delta\mathbf{W}_i$, and the merged weights by $\mathbf{W}_{\text{merge}}$. For LoRA task vectors, we write $\Delta\mathbf{W}_i = \mathbf{B}_i\mathbf{A}_i^\top$. The scaling coefficient for merging is denoted by λ . Our evaluation spans two distinct groups of baselines. *Vanilla merging* comprises (i) **RegMean** [40] aligns the merged model with fine-tuned models by solving a layer-wise least-squares problem using small calibration sets from each task, thereby matching the activations of the merged model to those of the task-specific models. (ii) **Task Arithmetic (TA)** [32] adds a scaled sum of task vectors to the pretrained weights, $\mathbf{W}_{\text{merge}} = \mathbf{W}_0 + \lambda \sum_{i=1}^N \Delta\mathbf{W}_i$. (iii) **TIES** [99] prunes small-magnitude parameters, resolves sign conflicts, and then averages only parameters with consistent signs with scaling coefficient λ . (iv) **DARE-TIES** [107] sparsifies each parameter with Bernoulli probability p and rescales the retained parameters by $1/(1-p)$ to preserve the expectation. (v) **AdaMerging** [101] learns merging coefficients by minimizing an output-entropy surrogate in the spirit of test-time adaptation [86]. *LoRA-aware merging* exploits low-rank adapter structure: (vi) **SVD** aggregates LoRA task vectors $\Delta\mathbf{W}_{\text{merge}} = \lambda \sum_i \mathbf{B}_i\mathbf{A}_i^\top$ and applies truncated SVD $\Delta\mathbf{W}_{\text{merge}} \approx \mathbf{U}_r\mathbf{\Sigma}_r\mathbf{V}_r^\top$ [84] to recover rank of original LoRAs (vii) **Linear** [59] performs TA on $\{\mathbf{B}_i\}$ and $\{\mathbf{A}_i\}$ rather than whole task vector. (viii) **KnOTS** [79] computes an SVD on concatenated task vectors $[\Delta\mathbf{W}_1; \dots; \Delta\mathbf{W}_N] = \mathbf{U}\mathbf{\Sigma}\mathbf{V}^\top$ and merge partitions of \mathbf{V} associated with each task vector. TIES or DARE-TIES can be applied to the \mathbf{V}_i , yielding the variants **KnOTS-TIES** and **KnOTS-DARE-TIES**. (ix) **LoRA-LEGO** [114] decomposes each adapter into minimal semantic units, clusters them rank-wise, and assembles a new LoRA from the cluster centroids. We present a reimplement of LoRA-LEGO. Finally, we also include the LoRA-aware (x) **RobustMerge** [109], and recent vanilla-merging methods: (xi) **EMR-Merging** [31], (xii) **FR-Merging** [115], and (xiii) **Iso-CTS** [60]. Implementation details are in Sec. C.3.

Implementation Details. For our method, we adopt AdamW [55] with a learning rate of 0.001. The direction-selection weights ϕ are initialized to 0.4 and optimized with a batch size of 16 for 500 iterations similar to Yang et al. [101] to control training cost. For experiments, we set $\alpha = 1$ in Eq. (16). The effects of α is analyzed in supple.

Metrics. Following prior work [32, 79, 99], we report the absolute accuracy of individually fine-tuned models on each dataset, and compare different merging methods using a normalized accuracy metric. The normalized accuracy is defined as $\frac{\text{Accuracy of merged model on task-}i}{\text{Accuracy of fine-tuned model on task-}i}$. This metric indicates how closely a merged model approaches the performance of the corresponding fine-tuned model for each task.

5.1. Experimental Results

Per-Task Evaluation across Vision Tasks. In this experiments, we adopt the conventional per-task evaluation protocol [32, 79, 99], where the goal is to test how well different merging strategies preserve task-specific performance. Concretely, a collection of models fine-tuned independently on separate datasets are merged into a unified model, and its performance is measured on each dataset separately, relying solely on the dataset’s own samples and labels. Table 1 reports normalized per-task accuracies and their averages across eight vision tasks with CLIP, where all models are fine-tuned with LoRA of rank 16. We categorize the baselines into two groups: vanilla merging methods and LoRA-aware methods that explicitly incorporate the LoRA structure. LoRA-aware methods generally outperform their vanilla counterparts. For instance, KnOTS-TIES surpasses TIES, and KnOTS-DARE-TIES improves upon DARE-TIES. KnOTS-based variants highlight the benefits of accounting for LoRA structure. LoRA-LEGO does not provide significant advantages over vanilla methods, suggesting that merely preserving LoRA rank-1 directions is insufficient to retain task-specific information during merging. By comparison, TARA consistently outperforms both vanilla and LoRA-aware baselines. Variant A shows steady gains with additional training iterations, leading to higher average accuracy. Variant B achieves the best overall trade-off, delivering the highest scores average of 76.3% with only 250 iterations. These results demonstrate that exploiting LoRA structure is essential for stable merging, and that TARA further effectively capture task-sensitive subspaces. Experiments in Table 1 use the checkpoints released by KnOTS [79]. We further confirm the results on independently trained checkpoints, as shown in Table 9.

Per-Task Evaluation on 6 NLI Tasks with LLMs. In Table 2, we report per-task normalized accuracies of merged models on six NLI benchmarks. For this setting, we apply six LoRA adapters with rank 16 to LLaMA-3-8B [19]. Each benchmark follows the natural language inference protocol, where a hypothesis is classified against a given premise into entailment, contradiction, or neutral. Detailed descriptions of each dataset are provided in Section C.1 of supplementary material.. The NLI results with LLMs reveal trends consistent with those observed in vision tasks. Vanilla merging baselines, with the exception of AdaMerging, show limited ability to preserve task-specific information in large-scale models, while LoRA-aware methods still provide only moderate improvements. In contrast, TARA delivers significant and consistent gains. Variant B achieving the best average normalized accuracy of 80.3%, highlighting the effectiveness of TARA on language tasks.

Joint-Task Evaluation of General Models. The joint-task evaluation protocol, originally introduced by Stoica et al.

Table 2. Per-task accuracy on six NLI benchmarks. We merge six LLaMA-3 8B checkpoints, each fine-tuned with LoRA. The upper panel shows the absolute per-task accuracy of the fine-tuned baselines. The lower panel shows the merged models’ accuracy, normalized by each task’s corresponding fine-tuned baseline (%).

Method	Dataset						Avg
	MNLI	QNLI	SNLI	RTE	SICK	SCITAIL	
<i>Per-task absolute accuracies (%)</i>							
Finetuned	90.8	95.3	92.1	84.8	91.3	87.3	90.2
<i>Per-task accuracies of merged models, normalized to finetuned (%)</i>							
Vanilla Merging							
TA [32]	67.3	87.3	41.8	95.7	77.9	76.9	74.6
TIES [99]	61.3	91.5	38.2	85.5	76.8	70.5	70.6
DARE-TIES [107]	42.0	72.5	44.1	77.8	76.9	86.8	66.7
EMR-Merging [31]	75.3	87.5	41.2	88.0	70.3	73.9	72.7
Iso-C [60]	35.0	57.8	40.5	64.1	51.1	100.2	58.1
Iso-CTS [60]	37.1	57.1	39.8	59.4	49.8	95.3	56.4
FR-Merging [115]	65.7	86.9	41.9	93.2	78.3	77.6	73.9
AdaMerging [101]	47.5	92.9	41.3	102.6	93.8	94.2	78.7
LoRA-aware Merging							
SVD [84]	67.7	87.2	41.7	95.7	77.6	76.6	74.4
Linear [59]	63.1	86.2	39.5	90.6	77.5	74.5	71.9
KnOTS-TIES [79]	41.1	83.4	56.6	87.2	87.9	94.8	75.2
KnOTS-DARE-TIES [79]	76.4	88.2	39.9	99.2	79.6	75.6	76.5
LoRA-LEGO [114]	62.5	84.8	41.4	100.0	87.0	83.7	76.6
RobustMerge [109]	66.4	87.2	41.8	94.0	77.7	77.3	74.1
TARA-Variant A	51.7	92.6	41.4	102.6	95.3	94.4	79.7
TARA-Variant B	46.8	94.1	41.4	103.4	98.1	97.8	80.3

Table 3. **Joint-Task Evaluation Results.** All models share a ViT-B/32 backbone, are fine-tuned with LoRA on separate datasets, and are then merged for joint-task evaluation.

Method	Hits@1	Hits@3	Hits@5
TA [32]	43.5	65.2	74.0
TIES [99]	43.6	65.3	73.9
DARE-TIES [107]	44.0	66.4	75.1
AdaMerging [101]	48.1	73.2	83.0
KnOTS-TIES [79]	46.8	68.1	76.3
KnOTS-DARE-TIES [79]	45.2	66.9	75.3
LoRA-LEGO [114]	43.1	65.0	73.9
TARA-Variant A	51.1	75.9	84.9
TARA-Variant B	49.3	74.9	85.1

[79], differs from the per-task setup by evaluating merged models over the union of inputs and labels from all eight vision benchmarks. This setting is more suitable for assessing whether a merged model can serve as a general-purpose model across multiple target datasets. In constructing the joint task, labels from all benchmarks are pooled together and duplicates are removed, resulting in a unified label space. A detailed description of this setting is provided in Section C.4 of supplementary material. Table 3 presents joint-task evaluation results in terms of top-1/3/5 accuracies. Vanilla merging baselines achieve limited performance with Hits@1 below 45%. KnOTS-TIES and KnOTS-DARE-TIES obtain small but consistent gains, while AdaMerging achieves further improvements when additional optimization iterations are allowed. TARA consistently outperforms all baselines. Both Variant A and Variant B benefit from longer training, with Variant A (500 Iters) reaching the highest Hits@1 (51.1%) and strong

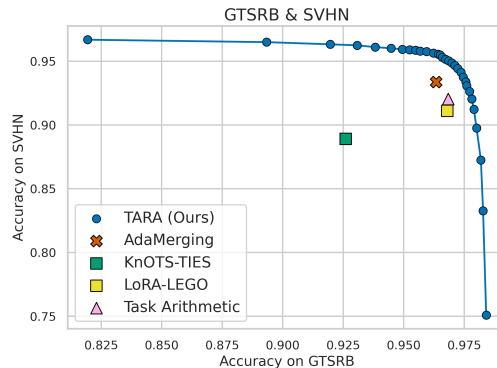


Figure 3. **Two-Task Merging Results.**

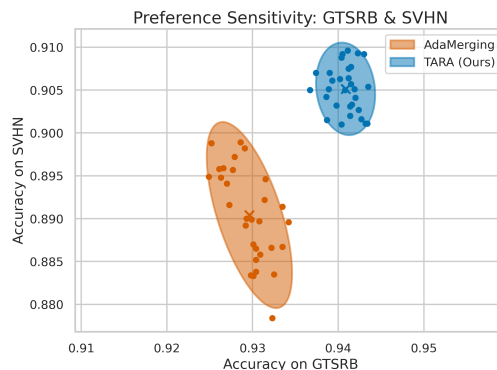


Figure 4. **Preference Sensitivity** of TARA and AdaMerging.

overall balance, while Variant B delivers the best Hits@5 (85.1%). These results highlight that our merging strategy effectively integrates task-specific knowledge across

Table 4. Generalization results on two unseen tasks when merging ViT-B/32 models on six tasks.

Method	Seen Tasks						Unseen Tasks			All Tasks	
	Cars	DTD	GTSRB	RESISC45	SUN397	SVHN	Avg Acc	EuroSAT	MNIST		Avg Acc
<i>Per-task accuracies of merged models, normalized to finetuned (%)</i>											
TA [32]	82.0	74.7	42.2	71.1	96.8	42.2	68.2	37.5	48.2	42.9	61.8
TIES [99]	81.5	73.2	40.3	64.4	95.4	45.7	66.7	37.2	61.8	49.5	62.4
KnOTS-TIES [79]	82.7	74.4	48.5	72.5	95.3	50.2	70.6	33.2	50.5	41.8	63.4
KnOTS-DARE-TIES [79]	81.7	72.5	49.4	71.9	94.6	52.5	70.4	31.6	51.2	41.4	63.2
LoRA-LEGO [114]	82.2	73.5	46.9	71.2	96.7	40.8	68.5	35.5	44.7	40.1	61.4
AdaMerging [101]	79.7	73.4	37.7	69.8	97.9	67.4	71.0	48.7	58.7	53.7	66.7
TARA-Variant A	82.8	73.9	43.8	70.5	98.2	73.4	73.8	48.4	61.1	54.8	69.1
TARA-Variant B	86.3	73.8	47.6	73.8	99.1	71.6	75.4	53.3	61.6	57.5	70.9
Method	Cars	DTD	EuroSAT	GTSRB	MNIST	SUN397	Avg Acc	RESISC45	SVHN	Avg Acc	Avg Acc
	<i>Per-task accuracies of merged models, normalized to finetuned (%)</i>										
TA [32]	82.3	75.1	53.0	40.7	52.4	96.7	66.7	68.6	34.7	51.7	63.0
TIES [99]	81.9	74.8	73.7	33.2	63.4	95.6	70.4	68.9	31.6	50.3	65.4
KnOTS-TIES [79]	82.5	72.9	53.8	47.8	61.7	94.9	69.0	67.5	35.1	51.3	64.5
KnOTS-DARE-TIES [79]	82.7	72.2	53.1	48.5	61.5	94.3	68.7	66.7	35.4	51.0	64.3
LoRA-LEGO [114]	81.1	72.3	55.6	42.8	62.6	94.7	68.2	65.2	33.9	49.5	63.5
AdaMerging [101]	79.6	74.2	72.5	36.5	60.0	97.9	70.1	69.2	41.1	55.2	66.4
TARA-Variant A	84.9	75.7	76.3	40.5	77.4	97.5	75.4	69.5	42.1	55.8	70.5
TARA-Variant B	86.7	77.0	79.5	42.8	76.3	98.2	76.8	70.5	45.6	58.1	72.1

datasets and yields more general models under the challenging joint-task setting. The full results are provided in Table 8 of supplementary material.

Two-Task Trade-Off Analysis. We examine whether preference-aware merging can trace an accuracy trade-off. Figure 3 shows results on the CLIP ViT-B/32 backbone. For the GTSRB-SVHN pair, sweeping 30 preference values and merging the two adapters with TARA yields a smooth trade-off curve (line). Baseline mergers (AdaMerging, KnOTS, LoRA-LEGO, TA) appear as isolated operating points. By jointly accounting for *subspace coverage* (retaining effective rank) and *anisotropy* (reweighting directional emphasis), TARA produces merged models that reflect diverse preferences and in turn typically lie above the baseline points, offering stronger accuracy trade-offs at comparable performance levels and enabling selection of an operating point by adjusting the preference.

Preference Sensitivity Analysis. To assess robustness to changes in the preference vector, we adopt the following setting. We fix the GTSRB and SVHN preferences to 0.125 each and randomly sample the remaining task preferences on the simplex so that all entries sum to 1. We sample 30 preference vectors and merge eight CLIP ViT-B/32 adapters with TARA and with AdaMerging, then record accuracies on GTSRB and SVHN. In Figure 4 each point corresponds to one sampled preference and its resulting two-task accuracies. For AdaMerging we use a weighted sum of per-task pseudo-objectives. Compared to AdaMerging, TARA produces a tighter point cloud with lower empirical covariance and more stable two-task performance under preference perturbations, consistent with its direction-aware handling during LoRA merging.

Evaluation of Generalization to Unseen Tasks. We assess the generalization performance of TARA following

the evaluation protocol of Yang et al. [101]. In this setting, *seen tasks* are those for which LoRA fine-tuned checkpoints are available and included during merging, whereas *unseen tasks* correspond to datasets without any associated LoRA checkpoints. As shown in Table 4, models are merged on six seen tasks and subsequently evaluated on both the seen tasks themselves and two unseen tasks. The results demonstrate that vanilla baselines and LoRA-aware methods struggle to achieve strong performance on unseen datasets. In contrast, TARA consistently outperforms all baselines across both evaluation groups. Variant B achieves the highest overall accuracy of 70.9% in the first split, while Variant B reaches 72.1% in the second split. These results show that TARA preserves in-domain performance and generalizes better to unseen benchmarks.

We provide more detailed analyses, including computational and memory costs, in Sec. F of the supplement.

6. Conclusion

We revisited LoRA merging through two complementary lenses: *subspace coverage*, where LoRA updates collectively occupy a wide, low-redundancy subspace rather than collapsing onto a few shared directions, and *anisotropy*, the directional imbalance in how changes in the scale of LoRA rank-1 directions translate into loss changes. Ignoring either can collapse useful subspaces and bias loss-critical directions. Building on effective-rank and directional-sensitivity analyses, we introduce TARA-Merging to align direction weights with task preferences while preserving task-relevant subspaces. Direction-wise reweighting maintains high subspace coverage and accounts for anisotropy, yielding consistent gains across per-task, joint, and transfer evaluations. This demonstrates that addressing both factors is key to robust, general-purpose LoRA merging.

Acknowledgements This research was supported by the Challengeable Future Defense Technology Research and Development Program through the Agency For Defense Development(ADD) funded by the Defense Acquisition Program Administration(DAPA) in 2026(No.915102201)

References

- [1] Samuel K Ainsworth, Jonathan Hayase, and Siddhartha Srinivasa. Git re-basin: Merging models modulo permutation symmetries. *arXiv preprint arXiv:2209.04836*, 2022. 2
- [2] Takuya Akiba, Makoto Shing, Yujin Tang, Qi Sun, and David Ha. Evolutionary optimization of model merging recipes. *Nature Machine Intelligence*, 7(2):195–204, 2025. 1
- [3] Luisa Bentivogli, Peter Clark, Ido Dagan, and Danilo Giampiccolo. The fifth pascal recognizing textual entailment challenge. *TAC*, 7(8):1, 2009. 2
- [4] Samuel R Bowman, Gabor Angeli, Christopher Potts, and Christopher D Manning. A large annotated corpus for learning natural language inference. *arXiv preprint arXiv:1508.05326*, 2015. 2
- [5] Hao Mark Chen, Shell Xu Hu, Wayne Luk, Timothy Hospedales, and Hongxiang Fan. Fw-merging: Scaling model merging with frank-wolfe optimization. In *Proceedings of the IEEE/CVF International Conference on Computer Vision*, pages 3390–3400, 2025. 13
- [6] Shiqi Chen, Jinghan Zhang, Tongyao Zhu, Wei Liu, Siyang Gao, Miao Xiong, Manling Li, and Junxian He. Bring reason to vision: Understanding perception and reasoning through model merging. In *Forty-second International Conference on Machine Learning*, 2025. 2
- [7] Weiyu Chen and James Kwok. Pareto merging: Multi-objective optimization for preference-aware model merging. *arXiv preprint arXiv:2408.12105*, 2024. 2
- [8] Gong Cheng, Junwei Han, and Xiaoqiang Lu. Remote sensing image scene classification: Benchmark and state of the art. *Proceedings of the IEEE*, 105(10):1865–1883, 2017. 2, 4
- [9] Runxi Cheng, Feng Xiong, Yongxian Wei, Wanyun Zhu, and Chun Yuan. Whoever started the interference should end it: Guiding data-free model merging via task vectors. *arXiv preprint arXiv:2503.08099*, 2025. 2
- [10] Mircea Cimpoi, Subhransu Maji, Iasonas Kokkinos, Sammy Mohamed, and Andrea Vedaldi. Describing textures in the wild. In *Proceedings of the IEEE conference on computer vision and pattern recognition*, pages 3606–3613, 2014. 2
- [11] Donato Crisostomi, Marco Fumero, Daniele Baieri, Florian Bernard, and Emanuele Rodola. C²M³: Cycle-consistent multi-model merging. *Advances in Neural Information Processing Systems*, 37:28674–28705, 2024. 1
- [12] Ido Dagan, Oren Glickman, and Bernardo Magnini. The pascal recognising textual entailment challenge. In *Machine learning challenges workshop*, pages 177–190. Springer, 2005. 2
- [13] Nico Daheim, Thomas Möllenhoff, Edoardo Maria Ponti, Iryna Gurevych, and Mohammad Emtiyaz Khan. Model merging by uncertainty-based gradient matching. *arXiv preprint arXiv:2310.12808*, 2023. 2
- [14] MohammadReza Davari and Eugene Belilovsky. Model breadcrumbs: Scaling multi-task model merging with sparse masks. In *European Conference on Computer Vision*, pages 270–287. Springer, 2024. 2
- [15] Pala Tej Deep, Rishabh Bhardwaj, and Soujanya Poria. Della-merging: Reducing interference in model merging through magnitude-based sampling. *arXiv preprint arXiv:2406.11617*, 2024. 1
- [16] Jia Deng, Wei Dong, Richard Socher, Li-Jia Li, Kai Li, and Li Fei-Fei. Imagenet: A large-scale hierarchical image database. In *2009 IEEE conference on computer vision and pattern recognition*, pages 248–255. Ieee, 2009. 5, 2
- [17] Alexey Dosovitskiy, Lucas Beyer, Alexander Kolesnikov, Dirk Weissenborn, Xiaohua Zhai, Thomas Unterthiner, Mostafa Dehghani, Matthias Minderer, Georg Heigold, Sylvain Gelly, et al. An image is worth 16x16 words: Transformers for image recognition at scale. *arXiv preprint arXiv:2010.11929*, 2020. 5
- [18] Yiyang Du, Xiaochen Wang, Chi Chen, Jiabo Ye, Yiru Wang, Peng Li, Ming Yan, Ji Zhang, Fei Huang, Zhifang Sui, et al. Adamms: Model merging for heterogeneous multimodal large language models with unsupervised coefficient optimization. In *Proceedings of the Computer Vision and Pattern Recognition Conference*, pages 9413–9422, 2025. 2
- [19] Abhimanyu Dubey, Abhinav Jauhri, Abhinav Pandey, Abhishek Kadian, Ahmad Al-Dahle, Aiesha Letman, Akhil Mathur, Alan Schelten, Amy Yang, Angela Fan, et al. The llama 3 herd of models. *arXiv e-prints*, pages arXiv–2407, 2024. 2, 5, 6, 3
- [20] Sebastian Dzia dzio, Vishaal Udandarao, Karsten Roth, Ameya Prabhu, Zeynep Akata, Samuel Albanie, and Matthias Bethge. How to merge your multimodal models over time? In *Proceedings of the IEEE/CVF Conference on Computer Vision and Pattern Recognition (CVPR)*, pages 20479–20491, 2025. 2
- [21] Rahim Entezari, Hanie Sedghi, Olga Saukh, and Behnam Neyshabur. The role of permutation invariance in linear mode connectivity of neural networks. *arXiv preprint arXiv:2110.06296*, 2021. 2
- [22] Rohit Gandikota, Joanna Materzyńska, Tingrui Zhou, Antonio Torralba, and David Bau. Concept sliders: Lora adapters for precise control in diffusion models. In *European Conference on Computer Vision*, pages 172–188. Springer, 2024. 2
- [23] Antonio Andrea Gargiulo, Donato Crisostomi, Maria Sofia Bucarelli, Simone Scardapane, Fabrizio Silvestri, and Emanuele Rodola. Task singular vectors: Reducing task interference in model merging. In *Proceedings of the Computer Vision and Pattern Recognition Conference*, pages 18695–18705, 2025. 2, 1
- [24] Danilo Giampiccolo, Bernardo Magnini, Ido Dagan, and William B Dolan. The third pascal recognizing textual entailment challenge. In *Proceedings of the ACL-PASCAL*

- workshop on textual entailment and paraphrasing*, pages 1–9, 2007. 2
- [25] Danna Gurari, Qing Li, Abigale J Stangl, Anhong Guo, Chi Lin, Kristen Grauman, Jiebo Luo, and Jeffrey P Bigham. Vizwiz grand challenge: Answering visual questions from blind people. In *Proceedings of the IEEE conference on computer vision and pattern recognition*, pages 3608–3617, 2018. 7
- [26] R Bar Haim, Ido Dagan, Bill Dolan, Lisa Ferro, Danilo Giampiccolo, Bernardo Magnini, and Idan Szpektor. The second pascal recognising textual entailment challenge. In *Proceedings of the Second PASCAL Challenges Workshop on Recognising Textual Entailment*, pages 785–794, 2006. 2
- [27] Patrick Helber, Benjamin Bischke, Andreas Dengel, and Damian Borth. Eurosat: A novel dataset and deep learning benchmark for land use and land cover classification. *IEEE Journal of Selected Topics in Applied Earth Observations and Remote Sensing*, 12(7):2217–2226, 2019. 2
- [28] Stefan Horoi, Guy Wolf, Eugene Belilovsky, and Gintare Karolina Dziugaite. Less is more: Undertraining experts improves model upcycling. *arXiv preprint arXiv:2506.14126*, 2025. 2
- [29] Edward J Hu, Yelong Shen, Phillip Wallis, Zeyuan Allen-Zhu, Yuanzhi Li, Shean Wang, Lu Wang, Weizhu Chen, et al. Lora: Low-rank adaptation of large language models. *ICLR*, 1(2):3, 2022. 1, 2, 3
- [30] Chengsong Huang, Qian Liu, Bill Yuchen Lin, Tianyu Pang, Chao Du, and Min Lin. Lorahub: Efficient cross-task generalization via dynamic lora composition. In *Conference on Language Modeling (COLM)*, 2024. 2
- [31] Chenyu Huang, Peng Ye, Tao Chen, Tong He, Xiangyu Yue, and Wanli Ouyang. Emr-merging: Tuning-free high-performance model merging. *Advances in Neural Information Processing Systems*, 37:122741–122769, 2024. 5, 6, 7, 1, 4
- [32] Gabriel Ilharco, Marco Tulio Ribeiro, Mitchell Wortsman, Suchin Gururangan, Ludwig Schmidt, Hannaneh Hajishirzi, and Ali Farhadi. Editing models with task arithmetic. *arXiv preprint arXiv:2212.04089*, 2022. 1, 2, 3, 4, 5, 6, 7, 8, 11, 12, 13
- [33] Moritz Imfeld, Jacopo Galdi, Marco Giordano, Thomas Hofmann, Sotiris Anagnostidis, and Sidak Pal Singh. Transformer fusion with optimal transport. *arXiv preprint arXiv:2310.05719*, 2023. 1
- [34] Arthur Jacot, Franck Gabriel, and Clément Hongler. Neural tangent kernel: Convergence and generalization in neural networks. *Advances in neural information processing systems*, 31, 2018. 1
- [35] Wooseong Jeong and Kuk-Jin Yoon. Quantifying task priority for multi-task optimization. In *Proceedings of the IEEE/CVF Conference on Computer Vision and Pattern Recognition*, pages 363–372, 2024. 1
- [36] Wooseong Jeong and Kuk-Jin Yoon. Resolving token-space gradient conflicts: Token space manipulation for transformer-based multi-task learning. In *Proceedings of the IEEE/CVF International Conference on Computer Vision*, pages 2887–2897, 2025.
- [37] Wooseong Jeong and Kuk-Jin Yoon. Selective task group updates for multi-task optimization. In *The Thirteenth International Conference on Learning Representations*, 2025.
- [38] Wooseong Jeong, Jegyeong Cho, Youngho Yoon, and Kuk-Jin Yoon. Synchronizing task behavior: Aligning multiple tasks during test-time training. In *Proceedings of the IEEE/CVF International Conference on Computer Vision*, pages 24340–24350, 2025. 1
- [39] Ruochen Jin, Bojian Hou, Jiancong Xiao, Weijie Su, and Li Shen. Fine-tuning linear layers only is a simple yet effective way for task arithmetic. *arXiv preprint arXiv:2407.07089*, 2024. 1
- [40] Xisen Jin, Xiang Ren, Daniel Preotiuc-Pietro, and Pengxiang Cheng. Dataless knowledge fusion by merging weights of language models. *arXiv preprint arXiv:2212.09849*, 2022. 2, 5, 6
- [41] Ege Kesim and Selahattin Serdar Helli. Multi lora meets vision: Merging multiple adapters to create a multi task model. *arXiv preprint arXiv:2411.14064*, 2024. 2
- [42] Tushar Khot, Ashish Sabharwal, and Peter Clark. Scitail: A textual entailment dataset from science question answering. In *Proceedings of the AAAI conference on artificial intelligence*, 2018. 2
- [43] Jonathan Krause, Michael Stark, Jia Deng, and Li Fei-Fei. 3d object representations for fine-grained categorization. In *Proceedings of the IEEE international conference on computer vision workshops*, pages 554–561, 2013. 2
- [44] Yann LeCun. The mnist database of handwritten digits. <http://yann.lecun.com/exdb/mnist/>, 1998. 2, 4
- [45] Giwon Lee, Wooseong Jeong, Daehee Park, Jaewoo Jeong, and Kuk-Jin Yoon. Interaction-merged motion planning: Effectively leveraging diverse motion datasets for robust planning. In *Proceedings of the IEEE/CVF International Conference on Computer Vision*, pages 28610–28621, 2025. 2
- [46] Sanwoo Lee, Jiahao Liu, Qifan Wang, Jingang Wang, Xunliang Cai, and Yunfang Wu. Dynamic fisher-weighted model merging via bayesian optimization. *arXiv preprint arXiv:2504.18992*, 2025. 1
- [47] Dengchun Li, Yingzi Ma, Naizheng Wang, Zhengmao Ye, Zhiyuan Cheng, Yinghao Tang, Yan Zhang, Lei Duan, Jie Zuo, Cal Yang, et al. Mixlora: Enhancing large language models fine-tuning with lora-based mixture of experts. *arXiv preprint arXiv:2404.15159*, 2024. 2
- [48] Mengqi Liao, Wei Chen, Junfeng Shen, Shengnan Guo, and Huaiyu Wan. Hmora: Making llms more effective with hierarchical mixture of lora experts. In *The Thirteenth International Conference on Learning Representations*, 2025. 2
- [49] Xi Lin, Xiaoyuan Zhang, Zhiyuan Yang, Fei Liu, Zhenkun Wang, and Qingfu Zhang. Smooth tchebycheff scalarization for multi-objective optimization. *arXiv preprint arXiv:2402.19078*, 2024. 2, 5
- [50] Haotian Liu, Chunyuan Li, Yuheng Li, and Yong Jae Lee. Improved baselines with visual instruction tuning, 2023. 7
- [51] Haotian Liu, Chunyuan Li, Qingyang Wu, and Yong Jae Lee. Visual instruction tuning, 2023. 7

- [52] Shuqi Liu, Han Wu, Bowei He, Xiongwei Han, Mingxuan Yuan, and Linqi Song. Sens-merging: Sensitivity-guided parameter balancing for merging large language models. *arXiv preprint arXiv:2502.12420*, 2025. 1
- [53] Tian Yu Liu, Aditya Golatkar, and Stefano Soatto. Tangent transformers for composition, privacy and removal. *arXiv preprint arXiv:2307.08122*, 2023. 1
- [54] Ilya Loshchilov and Frank Hutter. SGDR: Stochastic gradient descent with warm restarts. In *International Conference on Learning Representations*, 2017. 3
- [55] Ilya Loshchilov and Frank Hutter. Decoupled weight decay regularization. In *International Conference on Learning Representations*, 2019. 6, 3, 7
- [56] Pan Lu, Liang Qiu, Jiaqi Chen, Tony Xia, Yizhou Zhao, Wei Zhang, Zhou Yu, Xiaodan Liang, and Song-Chun Zhu. Iconqa: A new benchmark for abstract diagram understanding and visual language reasoning. In *The 35th Conference on Neural Information Processing Systems (NeurIPS) Track on Datasets and Benchmarks*, 2021. 7
- [57] Pan Lu, Swaroop Mishra, Tanglin Xia, Liang Qiu, Kai-Wei Chang, Song-Chun Zhu, Oyvind Tafjord, Peter Clark, and Ashwin Kalyan. Learn to explain: Multimodal reasoning via thought chains for science question answering. *Advances in Neural Information Processing Systems*, 35: 2507–2521, 2022. 7
- [58] Zhenyi Lu, Chenghao Fan, Wei Wei, Xiaoye Qu, Danyang Chen, and Yu Cheng. Twin-merging: Dynamic integration of modular expertise in model merging. *Advances in Neural Information Processing Systems*, 37:78905–78935, 2024. 2
- [59] Sourab Mangrulkar, Sylvain Gugger, Lysandre Debut, Younes Belkada, Sayak Paul, and Benjamin Bossan. PEFT: State-of-the-art parameter-efficient fine-tuning methods. <https://github.com/huggingface/peft>, 2022. 5, 6, 7, 11, 12
- [60] Daniel Marczak, Simone Magistri, Sebastian Cygert, Bartłomiej Twardowski, Andrew D Bagdanov, and Joost van de Weijer. No task left behind: Isotropic model merging with common and task-specific subspaces. *arXiv preprint arXiv:2502.04959*, 2025. 2, 5, 6, 7, 4
- [61] Marco Marelli, Luisa Bentivogli, Marco Baroni, Raffaella Bernardi, Stefano Menini, and Roberto Zamparelli. Semeval-2014 task 1: Evaluation of compositional distributional semantic models on full sentences through semantic relatedness and textual entailment. In *Proceedings of the 8th international workshop on semantic evaluation (SemEval 2014)*, pages 1–8, 2014. 2
- [62] Ahmed Masry, Do Xuan Long, Jia Qing Tan, Shafiq Joty, and Enamul Hoque. Chartqa: A benchmark for question answering about charts with visual and logical reasoning. *arXiv preprint arXiv:2203.10244*, 2022. 7
- [63] Michael S Matena and Colin A Raffel. Merging models with fisher-weighted averaging. *Advances in Neural Information Processing Systems*, 35:17703–17716, 2022. 2
- [64] Minesh Mathew, Dimosthenis Karatzas, and CV Jawahar. Docvqa: A dataset for vqa on document images. In *Proceedings of the IEEE/CVF winter conference on applications of computer vision*, pages 2200–2209, 2021. 7
- [65] Kaisa Miettinen. *Nonlinear multiobjective optimization*. Springer Science & Business Media, 1999. 3
- [66] Anshul Nasery, Jonathan Hayase, Pang Wei Koh, and Se-woong Oh. Pleas-merging models with permutations and least squares. In *Proceedings of the Computer Vision and Pattern Recognition Conference*, pages 30493–30502, 2025. 1
- [67] Amin Heyrani Nobari, Kaveh Alimohammadi, Ali ArjomandBigdeli, Akash Srivastava, Faez Ahmed, and Navid Azizan. Activation-informed merging of large language models. *arXiv preprint arXiv:2502.02421*, 2025. 1
- [68] Guillermo Ortiz-Jimenez, Alessandro Favero, and Pascal Frossard. Task arithmetic in the tangent space: Improved editing of pre-trained models. *Advances in Neural Information Processing Systems*, 36, 2024. 1
- [69] Aniello Panariello, Daniel Marczak, Simone Magistri, Angelo Porrello, Bartłomiej Twardowski, Andrew D Bagdanov, Simone Calderara, and Joost van de Weijer. Accurate and efficient low-rank model merging in core space. *arXiv preprint arXiv:2509.17786*, 2025. 1
- [70] Akshara Prabhakar, Yuanzhi Li, Karthik Narasimhan, Sham Kakade, Eran Malach, and Samy Jelassi. Lora soups: Merging lorae for practical skill composition tasks. *arXiv preprint arXiv:2410.13025*, 2024. 1
- [71] Zihuan Qiu, Lei Wang, Yang Cao, Runtong Zhang, Bing Su, Yi Xu, Fanman Meng, Linfeng Xu, Qingbo Wu, and Hongliang Li. Null-space filtering for data-free continual model merging: Preserving transparency, promoting fidelity. *arXiv preprint arXiv:2509.21413*, 2025. 2
- [72] Alec Radford, Jong Wook Kim, Chris Hallacy, Aditya Ramesh, Gabriel Goh, Sandhini Agarwal, Girish Sastry, Amanda Askell, Pamela Mishkin, Jack Clark, et al. Learning transferable visual models from natural language supervision. In *International conference on machine learning*, pages 8748–8763. Pmlr, 2021. 1, 5, 3
- [73] Olivier Roy and Martin Vetterli. The effective rank: A measure of effective dimensionality. In *2007 15th European signal processing conference*, pages 606–610. IEEE, 2007. 3
- [74] Olga Russakovsky, Jia Deng, Hao Su, Jonathan Krause, Sanjeev Satheesh, Sean Ma, Zhiheng Huang, Andrej Karpathy, Aditya Khosla, Michael Bernstein, Alexander C. Berg, and Li Fei-Fei. ImageNet Large Scale Visual Recognition Challenge. *International Journal of Computer Vision (IJCV)*, 115(3):211–252, 2015. 7
- [75] Viraj Shah, Nataniel Ruiz, Forrester Cole, Erika Lu, Svetlana Lazebnik, Yuanzhen Li, and Varun Jampani. Ziplora: Any subject in any style by effectively merging lorae. In *European Conference on Computer Vision*, pages 422–438. Springer, 2024. 2
- [76] Li Shen, Anke Tang, Enneng Yang, Guibing Guo, Yong Luo, Lefei Zhang, Xiaochun Cao, Bo Du, and Dacheng Tao. Efficient and effective weight-ensembling mixture of experts for multi-task model merging. *arXiv preprint arXiv:2410.21804*, 2024. 2
- [77] Johannes Stalkamp, Marc Schlipf, Jan Salmen, and Christian Igel. The german traffic sign recognition benchmark: a multi-class classification competition. In *The 2011*

- international joint conference on neural networks*, pages 1453–1460. IEEE, 2011. 2
- [78] George Stoica, Daniel Bolya, Jakob Bjorner, Pratik Ramesh, Taylor Hearn, and Judy Hoffman. Zipit! merging models from different tasks without training. *arXiv preprint arXiv:2305.03053*, 2023. 2
- [79] George Stoica, Pratik Ramesh, Boglarka Ecsedi, Leshem Choshen, and Judy Hoffman. Model merging with svd to tie the knots. In *Proceedings of the International Conference on Learning Representations (ICLR)*, 2025. 1, 2, 3, 5, 6, 7, 8, 4, 9, 11, 12
- [80] Derek Tam, Mohit Bansal, and Colin Raffel. Merging by matching models in task parameter subspaces. *arXiv preprint arXiv:2312.04339*, 2023. 2
- [81] Anke Tang, Li Shen, Yong Luo, Yibing Zhan, Han Hu, Bo Du, Yixin Chen, and Dacheng Tao. Parameter efficient multi-task model fusion with partial linearization. *arXiv preprint arXiv:2310.04742*, 2023. 1
- [82] Anke Tang, Li Shen, Yong Luo, Shuai Xie, Han Hu, Lefei Zhang, Bo Du, and Dacheng Tao. Smile: Zero-shot sparse mixture of low-rank experts construction from pre-trained foundation models. *arXiv preprint arXiv:2408.10174*, 2024. 2
- [83] Anke Tang, Enneng Yang, Li Shen, Yong Luo, Han Hu, Bo Du, and Dacheng Tao. Merging models on the fly without retraining: A sequential approach to scalable continual model merging. *arXiv preprint arXiv:2501.09522*, 2025. 2
- [84] Dennis Tang, Prateek Yadav, Yi-Lin Sung, Jaehong Yoon, and Mohit Bansal. Lora merging with svd: Understanding interference and preserving performance. In *ICML 2025 Workshop on Reliable and Responsible Foundation Models*, 2025. 2, 5, 6, 7, 11, 12
- [85] Alex Wang, Amanpreet Singh, Julian Michael, Felix Hill, Omer Levy, and Samuel Bowman. Glue: A multi-task benchmark and analysis platform for natural language understanding. In *Proceedings of the 2018 EMNLP Workshop BlackboxNLP: Analyzing and Interpreting Neural Networks for NLP*, pages 353–355, 2018. 2
- [86] Dequan Wang, Evan Shelhamer, Shaoteng Liu, Bruno Olshausen, and Trevor Darrell. Tent: Fully test-time adaptation by entropy minimization. *arXiv preprint arXiv:2006.10726*, 2020. 6
- [87] Ke Wang, Nikolaos Dimitriadis, Alessandro Favero, Guillermo Ortiz-Jimenez, Francois Fleuret, and Pascal Frossard. Lines: Post-training layer scaling prevents forgetting and enhances model merging. *arXiv preprint arXiv:2410.17146*, 2024. 2
- [88] Ke Wang, Nikolaos Dimitriadis, Guillermo Ortiz-Jimenez, Francois Fleuret, and Pascal Frossard. Localizing task information for improved model merging and compression. *arXiv preprint arXiv:2405.07813*, 2024. 2
- [89] Ke Wang, Yiming Qin, Nikolaos Dimitriadis, Alessandro Favero, and Pascal Frossard. Memoir: Lifelong model editing with minimal overwrite and informed retention for llms. In *Advances in Neural Information Processing Systems (NeurIPS)*, 2025. 2
- [90] Yongxian Wei, Runxi Cheng, Weike Jin, Enneng Yang, Li Shen, Lu Hou, Sinan Du, Chun Yuan, Xiaochun Cao, and Dacheng Tao. Unifying multimodal large language model capabilities and modalities via model merging. *arXiv preprint arXiv:2505.19892*, 2025. 2
- [91] Yongxian Wei, Anke Tang, Li Shen, Zixuan Hu, Chun Yuan, and Xiaochun Cao. Modeling multi-task model merging as adaptive projective gradient descent. In *Forty-second International Conference on Machine Learning*, 2025. 2
- [92] Adina Williams, Nikita Nangia, and Samuel Bowman. A broad-coverage challenge corpus for sentence understanding through inference. In *Proceedings of the 2018 Conference of the North American Chapter of the Association for Computational Linguistics: Human Language Technologies, Volume 1 (Long Papers)*, pages 1112–1122, 2018. 2
- [93] Mitchell Wortsman, Gabriel Ilharco, Samir Ya Gadre, Rebecca Roelofs, Raphael Gontijo-Lopes, Ari S Morcos, Hongseok Namkoong, Ali Farhadi, Yair Carmon, Simon Kornblith, et al. Model soups: averaging weights of multiple fine-tuned models improves accuracy without increasing inference time. In *International conference on machine learning*, pages 23965–23998. PMLR, 2022. 1
- [94] Mitchell Wortsman, Gabriel Ilharco, Jong Wook Kim, Mike Li, Simon Kornblith, Rebecca Roelofs, Raphael Gontijo Lopes, Hannaneh Hajishirzi, Ali Farhadi, Hongseok Namkoong, et al. Robust fine-tuning of zero-shot models. In *Proceedings of the IEEE/CVF conference on computer vision and pattern recognition*, pages 7959–7971, 2022. 1
- [95] Han Wu, Yuxuan Yao, Shuqi Liu, Zehua Liu, Xiaojin Fu, Xiongwei Han, Xing Li, Hui-Ling Zhen, Tao Zhong, and Mingxuan Yuan. Unlocking efficient long-to-short llm reasoning with model merging. *arXiv preprint arXiv:2503.20641*, 2025. 1
- [96] Xun Wu, Shaohan Huang, and Furu Wei. Mixture of lora experts. *arXiv preprint arXiv:2404.13628*, 2024. 2
- [97] Jianxiong Xiao, James Hays, Krista A Ehinger, Aude Oliva, and Antonio Torralba. Sun database: Large-scale scene recognition from abbey to zoo. In *2010 IEEE computer society conference on computer vision and pattern recognition*, pages 3485–3492. IEEE, 2010. 2, 4
- [98] Zhengqi Xu, Ke Yuan, Huiqiong Wang, Yong Wang, Mingli Song, and Jie Song. Training-free pretrained model merging. In *Proceedings of the IEEE/CVF Conference on Computer Vision and Pattern Recognition*, pages 5915–5925, 2024. 2
- [99] Prateek Yadav, Derek Tam, Leshem Choshen, Colin A Raffel, and Mohit Bansal. Ties-merging: Resolving interference when merging models. *Advances in Neural Information Processing Systems*, 36:7093–7115, 2023. 1, 2, 3, 5, 6, 7, 8, 11, 12
- [100] Kunda Yan, Min Zhang, Sen Cui, Qu Zikun, Bo Jiang, Feng Liu, and Changshui Zhang. CALM: Consensus-aware localized merging for multi-task learning. In *Forty-second International Conference on Machine Learning*, 2025. 13
- [101] Enneng Yang, Zhenyi Wang, Li Shen, Shiwei Liu, Guibing Guo, Xingwei Wang, and Dacheng Tao. Adamerging: Adaptive model merging for multi-task learning. *arXiv preprint arXiv:2310.02575*, 2023. 1, 2, 3, 4, 5, 6, 7, 8, 11, 12, 13

- [102] Enneng Yang, Li Shen, Guibing Guo, Xingwei Wang, Xiaochun Cao, Jie Zhang, and Dacheng Tao. Model merging in llms, mllms, and beyond: Methods, theories, applications and opportunities. *arXiv preprint arXiv:2408.07666*, 2024. 1, 2
- [103] Enneng Yang, Li Shen, Zhenyi Wang, Guibing Guo, Xiaojun Chen, Xingwei Wang, and Dacheng Tao. Representation surgery for multi-task model merging. *arXiv preprint arXiv:2402.02705*, 2024. 2
- [104] Enneng Yang, Li Shen, Zhenyi Wang, Guibing Guo, Xingwei Wang, Xiaocun Cao, Jie Zhang, and Dacheng Tao. Surgeryv2: Bridging the gap between model merging and multi-task learning with deep representation surgery. *arXiv preprint arXiv:2410.14389*, 2024. 2
- [105] Enneng Yang, Anke Tang, Li Shen, Guibing Guo, Xingwei Wang, Xiaochun Cao, and Jie Zhang. Continual model merging without data: Dual projections for balancing stability and plasticity. In *The Thirty-ninth Annual Conference on Neural Information Processing Systems*, 2025. 2
- [106] Yang Yang, Wen Wang, Liang Peng, Chaotian Song, Yao Chen, Hengjia Li, Xiaolong Yang, Qinglin Lu, Deng Cai, Boxi Wu, et al. Lora-composer: Leveraging low-rank adaptation for multi-concept customization in training-free diffusion models. *arXiv preprint arXiv:2403.11627*, 2024. 2
- [107] Le Yu, Bowen Yu, Haiyang Yu, Fei Huang, and Yongbin Li. Language models are super mario: Absorbing abilities from homologous models as a free lunch. In *Forty-first International Conference on Machine Learning*, 2024. 1, 2, 5, 6, 7, 3, 11, 12
- [108] Netzer Yuval. Reading digits in natural images with unsupervised feature learning. In *Proceedings of the NIPS Workshop on Deep Learning and Unsupervised Feature Learning*, 2011. 2, 4
- [109] Fanhu Zeng, Haiyang Guo, Fei Zhu, Li Shen, and Hao Tang. Parameter efficient merging for multimodal large language models with complementary parameter adaptation. *arXiv preprint arXiv:2502.17159*, 2025. 5, 6, 7, 2, 4
- [110] Binchi Zhang, Zaiyi Zheng, Zhengzhang Chen, and Jun-dong Li. Beyond the permutation symmetry of transformers: The role of rotation for model fusion. *arXiv preprint arXiv:2502.00264*, 2025. 2
- [111] Haobo Zhang and Jiayu Zhou. Unraveling lora interference: Orthogonal subspaces for robust model merging. *arXiv preprint arXiv:2505.22934*, 2025. 1
- [112] Jinghan Zhang, Junteng Liu, Junxian He, et al. Composing parameter-efficient modules with arithmetic operation. *Advances in Neural Information Processing Systems*, 36: 12589–12610, 2023. 1
- [113] Juzheng Zhang, Jiacheng You, Ashwinee Panda, and Tom Goldstein. Lori: Reducing cross-task interference in multi-task low-rank adaptation. *arXiv preprint arXiv:2504.07448*, 2025. 1
- [114] Ziyu Zhao, Tao Shen, Didi Zhu, Zexi Li, Jing Su, Xuwu Wang, Kun Kuang, and Fei Wu. Merging loras like playing lego: Pushing the modularity of lora to extremes through rank-wise clustering. In *Proceedings of the International Conference on Learning Representations (ICLR)*, 2025. 1, 2, 5, 6, 7, 8, 3, 11, 12
- [115] Shenghe Zheng and Hongzhi Wang. Free-merging: Fourier transform for efficient model merging. In *Proceedings of the IEEE/CVF International Conference on Computer Vision*, pages 3863–3873, 2025. 5, 6, 7, 4
- [116] Shenghe Zheng, Hongzhi Wang, Chenyu Huang, Xiaohui Wang, Tao Chen, Jiayuan Fan, Shuyue Hu, and Peng Ye. Decouple and orthogonalize: A data-free framework for lora merging. *arXiv preprint arXiv:2505.15875*, 2025. 1
- [117] Ming Zhong, Yelong Shen, Shuohang Wang, Yadong Lu, Yizhu Jiao, Siru Ouyang, Donghan Yu, Jiawei Han, and Weizhu Chen. Multi-lora composition for image generation. *arXiv preprint arXiv:2402.16843*, 2024. 2
- [118] Yuyan Zhou, Liang Song, Bingning Wang, and Weipeng Chen. Metagpt: Merging large language models using model exclusive task arithmetic. *arXiv preprint arXiv:2406.11385*, 2024. 2
- [119] Didi Zhu, Yibing Song, Tao Shen, Ziyu Zhao, Jinluan Yang, Min Zhang, and Chao Wu. REMEDY: Recipe merging dynamics in large vision-language models. In *The Thirteenth International Conference on Learning Representations*, 2025. 2
- [120] Shaobin Zhuang, Yiwei Guo, Yanbo Ding, Kunchang Li, Xinyuan Chen, Yaohui Wang, Fangyikang Wang, Ying Zhang, Chen Li, and Yali Wang. Timestep master: Asymmetrical mixture of timestep lora experts for versatile and efficient diffusion models in vision. *arXiv preprint arXiv:2503.07416*, 2025. 2
- [121] Zhan Zhuang, Xiequn Wang, Wei Li, Yulong Zhang, Qiushi Huang, Shuhao Chen, Xuehao Wang, Yanbin Wei, Yuhe Nie, Kede Ma, Yu Zhang, and Ying Wei. Come together, but not right now: A progressive strategy to boost low-rank adaptation. In *Forty-second International Conference on Machine Learning*, 2025. 1
- [122] Xiandong Zou, Mingzhu Shen, Christos-Savvas Bouganis, and Yiren Zhao. Cached multi-lora composition for multi-concept image generation. *arXiv preprint arXiv:2502.04923*, 2025. 2

Preference-Aligned LoRA Merging: Preserving Subspace Coverage and Addressing Directional Anisotropy

Supplementary Material

A. Proof of Proposition 1

Proposition 1 (Anisotropy Bounds). *Let $\sigma_{\max}(\mathbf{J})$ and $\sigma_{\min}(\mathbf{J})$ denote the largest and smallest singular values of \mathbf{J} . Then, for any coefficient vector ϕ ,*

$$\sigma_{\min}(\mathbf{J}) \|\phi\|_2 \leq \|\mathbf{J}\phi\|_2 = \|\Delta\mathbf{f}\|_2 \leq \sigma_{\max}(\mathbf{J}) \|\phi\|_2. \quad (5)$$

When $\kappa(\mathbf{J}) = \sigma_{\max}(\mathbf{J})/\sigma_{\min}(\mathbf{J})$ is large, the map $\phi \mapsto \Delta\mathbf{f}$ is anisotropic, and equal-norm LoRA-direction updates need not yield proportional task-loss changes.

Proof. Let $\mathbf{J} \in \mathbb{R}^{N \times K}$ be the restricted task-loss Jacobian with entries $\mathbf{J}_{i,k} = \langle \nabla f_i(\mathbf{W}), \mathbf{S}_k \rangle$, and take its SVD $\mathbf{J} = \mathbf{U}\mathbf{\Sigma}\mathbf{V}^\top$, where $\mathbf{U} \in \mathbb{R}^{N \times q}$ and $\mathbf{V} \in \mathbb{R}^{K \times q}$ have orthonormal columns ($\mathbf{U}^\top\mathbf{U} = \mathbf{V}^\top\mathbf{V} = \mathbf{I}_q$), $\mathbf{\Sigma} = \text{diag}(\sigma_1, \dots, \sigma_q)$ with $\sigma_1 \geq \dots \geq \sigma_q > 0$, and $q = \text{rank}(\mathbf{J})$. For any coefficient vector $\phi \in \mathbb{R}^K$, define $\tilde{\phi} = \mathbf{V}^\top\phi \in \mathbb{R}^q$. By orthogonal invariance of the Euclidean norm,

$$\|\mathbf{J}\phi\|_2 = \|\mathbf{U}\mathbf{\Sigma}\mathbf{V}^\top\phi\|_2 = \|\mathbf{\Sigma}\mathbf{V}^\top\phi\|_2 = \|\mathbf{\Sigma}\tilde{\phi}\|_2. \quad (17)$$

The second equality holds since multiplication by \mathbf{U} preserves the ℓ_2 norm: for any $y \in \mathbb{R}^q$, $\|\mathbf{U}y\|_2 = \|y\|_2$. Also, because \mathbf{V} has orthonormal columns, $\|\mathbf{V}^\top\phi\|_2 \leq \|\phi\|_2$.

Since $\mathbf{\Sigma}$ is diagonal,

$$\|\mathbf{J}\phi\|_2^2 = \|\mathbf{\Sigma}\tilde{\phi}\|_2^2 = \sum_{i=1}^q \sigma_i^2 \tilde{\phi}_i^2. \quad (18)$$

For the upper bound, use $\sigma_i \leq \sigma_{\max}(\mathbf{J})$ and $\|\tilde{\phi}\|_2 \leq \|\phi\|_2$ to obtain

$$\|\mathbf{J}\phi\|_2^2 = \sum_{i=1}^q \sigma_i^2 \tilde{\phi}_i^2 \leq \sigma_{\max}(\mathbf{J})^2 \sum_{i=1}^q \tilde{\phi}_i^2 \leq \sigma_{\max}(\mathbf{J})^2 \|\phi\|_2^2, \quad (19)$$

hence $\|\mathbf{J}\phi\|_2 \leq \sigma_{\max}(\mathbf{J}) \|\phi\|_2$.

For the lower bound, decompose $\phi = \phi_{\text{R}} + \phi_{\text{N}}$ with $\phi_{\text{R}} := \mathbf{V}\mathbf{V}^\top\phi \in \text{range}(\mathbf{V})$ and $\phi_{\text{N}} := (\mathbf{I} - \mathbf{V}\mathbf{V}^\top)\phi \in \text{ker}(\mathbf{J})$. Equivalently, $\tilde{\phi} = (\tilde{\phi}_1, \dots, \tilde{\phi}_q)$ are the coordinates of ϕ_{R} in the \mathbf{V} -basis. Then

$$\|\mathbf{J}\phi\|_2^2 = \sum_{i=1}^q \sigma_i^2 \tilde{\phi}_i^2 \geq \sigma_{\min}(\mathbf{J})^2 \sum_{i=1}^q \tilde{\phi}_i^2 = \sigma_{\min}(\mathbf{J})^2 \|\phi_{\text{R}}\|_2^2, \quad (20)$$

which implies $\|\mathbf{J}\phi\|_2 \geq \sigma_{\min}(\mathbf{J}) \|\phi_{\text{R}}\|_2$. If one restricts to the admissible subspace that excludes the nullspace (e.g.,

the LoRA span intersected with $\text{ker}(\mathbf{J})^\perp$), then $\phi_{\text{N}} = 0$ and $\|\phi_{\text{R}}\|_2 = \|\phi\|_2$, yielding

$$\sigma_{\min}(\mathbf{J}) \|\phi\|_2 \leq \|\mathbf{J}\phi\|_2 \leq \sigma_{\max}(\mathbf{J}) \|\phi\|_2.$$

(Equivalently, interpret $\sigma_{\min}(\mathbf{J})$ as the smallest *nonzero* singular value on the feasible subspace.) \square

B. Additional Related Work

Pre-Merging and Additional Model Merging. Pre-merging studies [81, 111, 113, 121] clarify and formalize the linear-composition behavior that *Task Arithmetic* relies on: they analyze when parameter-space combinations approximate joint training via partial or tangent linearization [39, 53, 68, 81] and connect these to NTK-style local linearization [34]. Building on this foundation, recent formulations explore optimal-transport fusion for Transformers [33], cycle-consistent multi-model merging [11], deriving layer-wise coefficients from model-internal statistics [31], permutation with least-squares alignment [66], constructing merging recipes from collections of fine-tuned models with diverse hyperparameters [93] with early evidence on CLIP that averaging robustness-oriented fine-tunes can improve zero-shot robustness [94], evolutionary search for recipe discovery [2], sparsity- and magnitude-aware sampling to reduce interference [15], and dynamic Fisher weighting guided by Bayesian optimization [46]. AIM [67] uses the information from the activation space of LLMs for merging. Another line of work leverages intermediate activations during inference or training and uses feature responses in specific layers to guide the merging process [52, 67, 95].

Additional LoRA-targeted Merging. Within *LoRA-targeted* methods, a training-free framework decouples direction and scale and orthogonalizes adapter directions before merging [116]. Zhang et al. [112] compose PEFT modules via weight-space arithmetic, enabling flexible transfer without extra training. Zhang and Zhou [111] enforce orthogonal LoRA subspaces pre-finetuning, reducing interference and preserving merge performance. Liu et al. [52] adjusts task and layer-wise merging coefficients using activation/gradient sensitivity and cross-task transferability. Several methods directly exploit low-rank structure for merging [23, 69, 70]. In particular, Panariello et al. [69] propose a core space that can be efficiently combined with existing merging baselines.

Model Merging in LLMs and VLMs. More recent work on model merging directly targets LLMs and VLMs and proposes strategies tailored to these architectures [6, 18, 58, 90, 109, 118, 119]. In particular, RobustMerge [109] introduces a merging method for MLLMs that exploits directional robustness in a low-rank space. Zhang et al. [110] leverage the rotation symmetry of self-attention layers, which substantially enlarges the equivalence set of Transformer models compared to permutation-based symmetries.

Model Merging for Multi-Task and Continual Learning.

Another line of work explicitly connects model merging with conventional multi-task learning [45, 76, 91, 103, 104], viewing merging as a mechanism for parameter sharing and representation consolidation across tasks. A complementary set of studies aims to localize task-specific information in the parameters or to quantify interference within linear layers [9, 14, 80, 88], while Marczak et al. [60] further decompose the parameter space into shared and task-specific subspaces. MuDSC [98] also explores heterogeneous settings with diverse dense prediction tasks for evaluating merging performance. However, it is not directly comparable to our setting because it allows branch-like architectures such as ZipIt [78]. Model merging has also been studied in continual learning scenarios [20, 71, 83, 87, 89, 105], where merging is used to mitigate catastrophic forgetting and to accumulate knowledge across tasks over time.

LoRA Composition. Dynamic routing or mixture-of-experts compositions learn to combine multiple LoRAs at inference time [47, 48, 82, 96], and few-shot dynamic composition improves cross-task transfer [28, 30]. In vision, multi-LoRA merging for multi-task recognition demonstrates modularity [41]. In diffusion, multi-LoRA composition and subject-style concept mixing further highlight modularity [22, 75, 106, 117, 120, 122]. These methods dynamically assign or route adapters per input or task in an MoE-like fashion, which alters the inference-time architecture and falls outside our scope.

C. Experimental Settings

C.1. Datasets

C.1.1. Vision Benchmarks

Following Stoica et al. [79], we adopt a ViT-B/32 backbone pre-trained on ImageNet-21k [16], fine-tuned with LoRA rank 16. Evaluation is conducted on eight standard image-classification datasets. Brief summaries are provided below.

SUN397 [97]. Large-scale scene recognition dataset with 397 categories and 108,754 images, each class having at least 100 samples.

Cars [43]. Fine-grained car recognition covering 196 categories with 16,185 images, evenly split into train and test.

RESISC45 [8]. Remote sensing benchmark with 45 scene classes and 31,500 images, about 700 per class.

EuroSAT [27]. Satellite image classification dataset of 27,000 images in 10 land-use categories across diverse regions.

SVHN [108]. Street View House Numbers dataset with 10 digit classes, 73,257 train images, 26,032 test images, and 500k+ extra samples.

GTSRB [77]. Traffic sign recognition dataset with 43 categories and over 50,000 labeled images.

MNIST [44]. Classic handwritten digit dataset of 70,000 grayscale images evenly distributed across 10 classes (60k train / 10k test).

DTD [10]. Texture classification dataset with 47 attributes and 5,640 images, about 120 per class.

C.1.2. Language Benchmarks

In addition to the main benchmarks used in the paper, we evaluate our method on six classification datasets to assess its applicability to large language models. These datasets are used in conjunction with the LLaMA-3 8B model. Below, we briefly summarize each dataset.

QNLI [85]. A question-answering dataset reformulated as sentence-pair classification. Each example is a (question, sentence) pair, and the label indicates whether the sentence contains the answer to the question (binary).

MNLI [92]. A large, crowdsourced collection of sentence pairs annotated for natural language inference. Given a premise and a hypothesis, the task is to predict one of three labels: *entailment*, *contradiction*, or *neutral* (three-class).

SNLI [4]. A corpus of ~570k human-written sentence pairs labeled for *entailment*, *contradiction*, or *neutral*, supporting the standard NLI task (three-class).

RTE [3, 12, 24, 26]. A suite of textual entailment datasets compiled from the RTE1, RTE2, RTE3, and RTE5 challenges. Examples are drawn from news and Wikipedia. In the GLUE formulation, all RTE sets are converted to binary classification by collapsing *neutral* and *contradiction* into *not-entailment* for consistency.

SICK [61]. A dataset of around 10k sentence pairs built from image and video captions. Each pair is labeled for semantic relatedness (1-5 scale) and for textual entailment with three classes: *entailment*, *contradiction*, and *neutral*. It is widely used for evaluating compositional semantics, entailment, and similarity in a unified setting.

SciTail [42]. An entailment dataset derived from multiple-choice science exams and web sentences. Each (premise, hypothesis) pair is labeled as *entails* or *neutral* (binary). The dataset contains 27,026 examples (10,101 *entails* and 16,925 *neutral*).

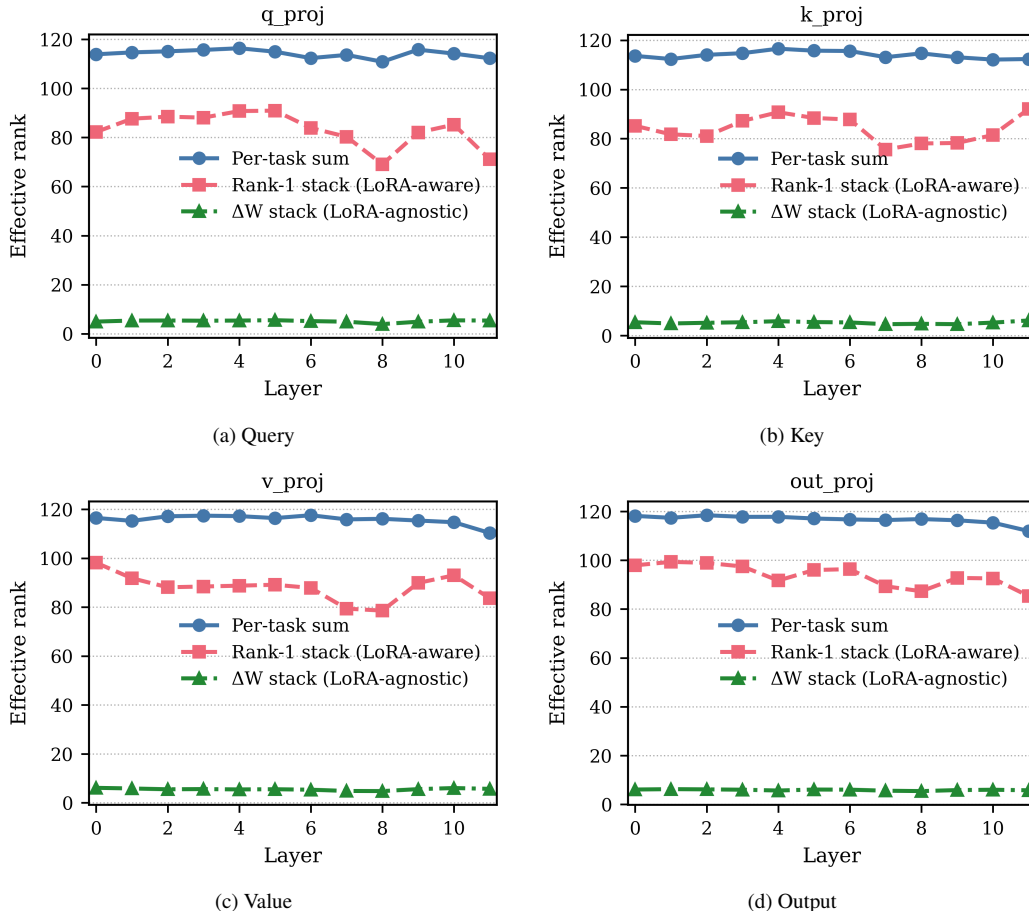


Figure 5. **Effective Rank** across layers for each module. Higher curves indicate broader subspace coverage. The gap between ΔW stack and Rank-1 stack reflects merge-induced collapse.

C.2. Training Details

For the vision tasks, we fine-tuned CLIP [72] with a ViT-B/32 backbone. All models were optimized using AdamW [55] with a learning rate of $3e-4$ and a cosine learning rate scheduler [54] with a weight decay of $1e-4$.

For sequence classification, we fine-tuned LLaMA-3 [19] with 8B parameters, following the setup of [79]. Optimization used AdamW with a learning rate of $3e-5$ and a linear scheduler. A linear classification head with three outputs was added for natural language inference (entailment, contradiction, neutral), and in binary settings predictions for the unused class were disregarded.

To enable efficient adaptation, we applied LoRA [29] to both CLIP and LLaMA. Specifically, low-rank adapters were attached to the query, key, value, and output projection matrices of each transformer block. Unless otherwise stated, the default LoRA hyperparameters were: rank = 16, $\alpha = 16$, and dropout = 0.1.

C.3. Implementation Details

In this paper, we compare our approach against ten baselines, following the experimental protocols reported in their original works. For TA [32], we tune the scaling coefficient of task vectors across the range of $[0.1, 0.2, \dots, 1.0]$. For TIES [99] and DARE-TIES [107], both the scaling coefficient λ and pruning coefficient η were selected via grid search. Specifically, λ was varied over $[0.8, 0.9, \dots, 1.8]$, while η was explored over $[0.1, 0.2, \dots, 0.9]$. For AdaMerging [101], all coefficients $\{\lambda_k^l\}_{n=1, l=1}^{N, L}$ (where N is the number of tasks and L the number of layers) are initialized to 0.3 before optimization with the entropy surrogate. For KnOTS [79], we evaluate two variants: KnOTS-TIES and KnOTS-DARE-TIES, which combine KnOTS with TIES [99] and DARE [107], respectively. For LoRA-LEGO [114], we reimplement the algorithm following the original paper. We apply k -means clustering to LoRA Minimal Semantic Units (MSUs), where each MSU $u = [a, b]$ consists of a row a from the LoRA down-projection matrix A and the corresponding

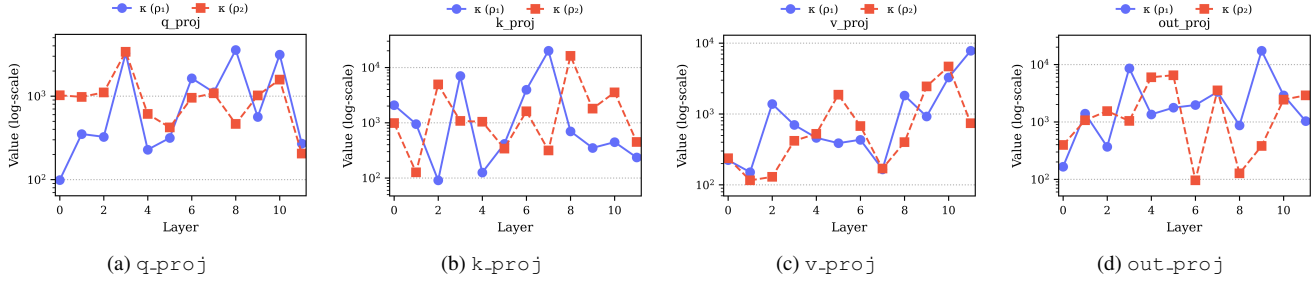


Figure 6. **Condition Number Anisotropy κ (RAW Basis)**. Layer-wise condition number $\kappa(\rho)$ per module under the non-orthogonal LoRA basis (RAW). Larger κ indicates stronger *within-preference* directional concentration of loss sensitivity. (Here, ρ_1 uniformly weights all tasks, whereas ρ_2 assigns all weight to a single task (one-hot).)

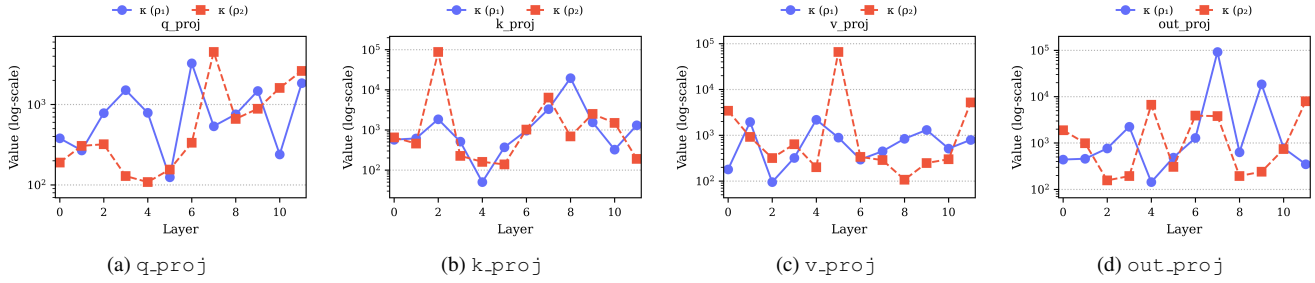


Figure 7. **Condition Number Anisotropy κ (SVD Basis)**. Layer-wise condition number $\kappa(\rho)$ per module under the orthogonal LoRA basis (SVD). Larger κ indicates stronger *within-preference* directional concentration of loss sensitivity. (Here, ρ_1 uniformly weights all tasks, whereas ρ_2 assigns all weight to a single task (one-hot).)

column b from the up-projection matrix B . We experiment with cluster sizes $k \in \{8, 16, 32, 64, 128\}$, and reproduce the dual scaling strategies: parameter reweighting and output reweighting. Parameter reweighting rescales each cluster centroid μ to match the average norm of its members, $\mu' = \frac{1}{p} \frac{\sum_{i=1}^p \|s_i\|}{\|\mu\|} \mu$, compensating for the reduced norm after merging, while output reweighting scales the merged LoRA by $\frac{\sqrt{r}}{\sqrt{k}}$ (with r the original LoRA rank and k the merged rank) to stabilize variance. We evaluate every k and both scaling strategies, reporting the best performance. We further include the LoRA-aware RobustMerge [109] and strong vanilla-merging methods EMR-Merging [31], FR-Merging [115], and Iso-CTS [60], and report their results in Sec. F.

C.4. Per-Task and Joint-Task Evaluation

In addition to the standard per-task benchmark, we also adopt the “joint-task” evaluation introduced by Stoica et al. [79]. Unlike the per-task regime, where each dataset is treated independently, the joint-task aggregates the inputs and labels from all eight vision benchmarks into a single evaluation pool. After combining all label sets, duplicate classes are removed (for example, MNIST [44] and SVHN [108] share the same digit categories), resulting in 748 unique labels across the combined benchmark. This

setup is particularly demanding because models must not only generalize within a task, but also discriminate among labels that appear across different datasets. In some cases, labels are semantically close or hierarchical, such as “islet” in SUN397 [97] and “island” in RESISC45 [8], which increases the difficulty of classification. To account for such ambiguity, evaluation is reported using Hits@ k metrics, where Hits@1 corresponds to top-1 accuracy and higher k values allow partial credit when the correct label appears among the top- k predictions. Joint-task protocol serves as an important benchmark for assessing the generality of merged models, as it directly tests whether a single model can operate across the diverse label space of multiple datasets.

D. Additional Analysis: Subspace Coverage

This appendix presents the exact formulations used in the main paper’s subspace-coverage analysis. We form all stacks by vectorizing matrices and placing one vector per row. Let $\mathbf{W}_0 \in \mathbb{R}^{d \times m}$ be the pre-trained weight. For task $i \in \{1, \dots, N\}$ with LoRA rank r_i , write $\Delta \mathbf{W}_i = \sum_{j=1}^{r_i} \mathbf{b}_{ij} \mathbf{a}_{ij}^\top$ with $\mathbf{b}_{ij} \in \mathbb{R}^d$ and $\mathbf{a}_{ij} \in \mathbb{R}^m$. Let $\text{vec}(\cdot) : \mathbb{R}^{d \times m} \rightarrow \mathbb{R}^{dm}$ denote matrix vectorization. For any matrix \mathbf{X} , let $\{\sigma_k\}_{k=1}^{R_{\mathbf{X}}}$ be its nonzero singular values with

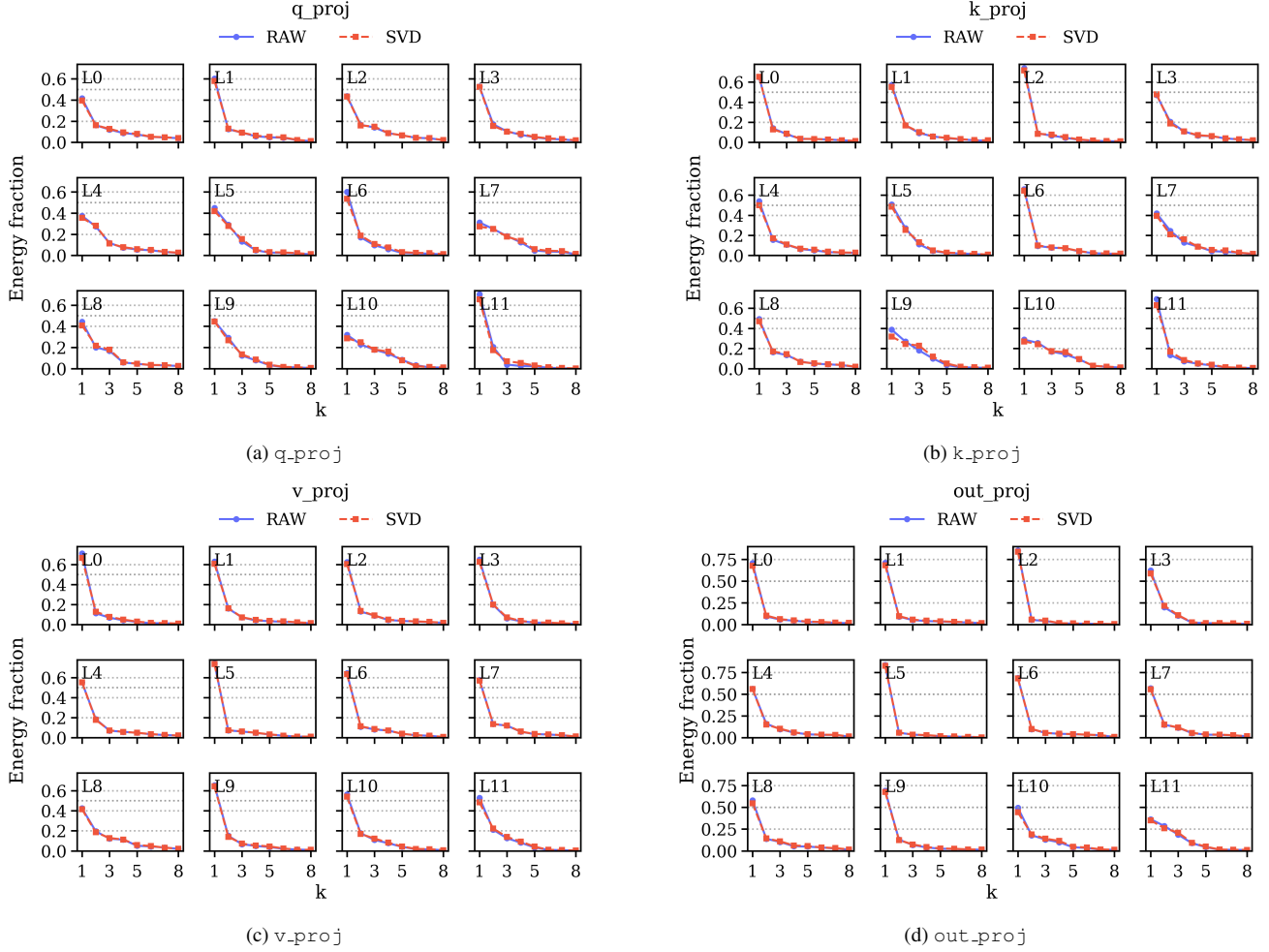


Figure 8. **Layer-wise Directional-Sensitivity Spectra (RAW vs. SVD)**. For each module and layer, we form the task-direction sensitivity matrix with entries $J_{i,k} = \langle \nabla f_i(W), S_k \rangle$ and plot the scree curve of its singular values as energy fractions $\sigma_k^2 / \sum_j \sigma_j^2$ versus component index k . “RAW” stacks rank-1 LoRA factors directly, while “SVD” uses a shared orthonormal basis. The two spectra are overlaid in each panel. A larger leading mass indicates stronger concentration of sensitivity into a few modes, whereas flatter spectra indicate a more distributed use of LoRA directions.

$R_{\mathbf{X}} = \text{rank}(\mathbf{X})$ and define

$$p_k = \frac{\sigma_k^2}{\sum_{j=1}^{R_{\mathbf{X}}} \sigma_j^2}, \quad \text{erank}(\mathbf{X}) = \exp\left(-\sum_{k=1}^{R_{\mathbf{X}}} p_k \log p_k\right).$$

The following entries are used in our analysis. For each entity, we define the stacked matrix and report its subspace coverage via effective rank.

- **Per-task sum** — compute coverage per task and then aggregate across tasks:

$$\mathbf{X}_i = \begin{bmatrix} \text{vec}(\mathbf{b}_{i1} \mathbf{a}_{i1}^\top) \\ \vdots \\ \text{vec}(\mathbf{b}_{ir_i} \mathbf{a}_{ir_i}^\top) \end{bmatrix} \in \mathbb{R}^{r_i \times dm},$$

$$\text{PerTaskSum} = \sum_{i=1}^N \text{erank}(\mathbf{X}_i).$$

- **ΔW stack (LoRA-agnostic)** — coverage of task updates when the LoRA rank-1 structure is ignored. We stack the task updates and use $\text{erank}(\mathbf{X}_{\text{agnostic}})$ with

$$\mathbf{X}_{\text{agnostic}} = \begin{bmatrix} \text{vec}(\Delta \mathbf{W}_1) \\ \vdots \\ \text{vec}(\Delta \mathbf{W}_N) \end{bmatrix} \in \mathbb{R}^{N \times dm},$$

- **Rank-1 stack (LoRA-aware)** — coverage when rank-1 directions from all adapters are retained. We stack all rank-1 directions and use $\text{erank}(\mathbf{X}_{\text{aware}})$ with

$$\mathbf{X}_{\text{aware}} = \begin{bmatrix} \text{vec}(\mathbf{b}_{11} \mathbf{a}_{11}^\top) \\ \vdots \\ \text{vec}(\mathbf{b}_{Nr_N} \mathbf{a}_{Nr_N}^\top) \end{bmatrix} \in \mathbb{R}^{(\sum_i r_i) \times dm},$$

Other modules. Supplementary results in Fig. 5 show the same qualitative pattern across additional modules (e.g., Attention and MLP layers). The ordering $\text{Per-task sum} \geq \text{Rank-1 stack (LoRA-aware)} \geq \Delta\mathbf{W} \text{ stack (LoRA-agnostic)}$ consistently holds, and the LoRA-aware stack retains roughly 60%~70% of the per-task sum. The gap between LoRA-aware and LoRA-agnostic reflects subspace collapse under interpolation-based merging.

E. Additional Analysis: Anisotropy

Within-Preference Anisotropy. We measure how unevenly a single preference $\rho \in \Delta_{N-1}$ concentrates loss sensitivity onto LoRA directions. Let $g(\rho; \mathbf{W}) = \sum_{i=1}^N \rho_i \nabla f_i(\mathbf{W})$ be the scalarized gradient at parameters \mathbf{W} obtained by *averaging* task LoRA updates and then scaling by 0.3 (as Task Arithmetic [32]). Given a basis of LoRA directions $\{\mathbf{S}_k\}_{k=1}^K$ (either the RAW stack of rank-1 factors or the shared SVD-orthonormal basis), define the directional sensitivities with *condition-number*. Larger κ indicates stronger *within-preference* concentration of sensitivity onto a few directions (greater anisotropy), while smaller κ indicates a more balanced use of the LoRA subspace. We report layer-wise $\kappa(\rho; \mathbf{W})$ for each module (q_proj, k_proj, v_proj, out_proj) under both RAW and SVD bases in Fig. 6 and Fig. 7. Here, ρ_1 uniformly weights all tasks, whereas ρ_2 assigns all weight to a single task (one-hot).

Figure 8 compares, for each module and layer, the singular-value energy distribution of the task-direction sensitivity matrix under the RAW (rank-1 factor stack) and SVD (shared orthonormal) bases. Each curve shows the energy fraction $\sigma_k^2 / \sum_j \sigma_j^2$ versus component index k . A larger leading mass indicates stronger anisotropy with sensitivity concentrated in a few directions, while flatter curves indicate a more balanced use of the LoRA subspace.

Directional-Sensitivity Misalignment in the SVD Basis.

Following Sec. 3.3, we conduct the same analysis with directional sensitivities projected onto the rank-1 LoRA directions obtained by SVD orthogonalization. We then compute a misalignment index $\xi(\rho_1, \rho_2)$ between the uniform and one-hot preferences across the LoRA layers. As shown in Fig. 9, the resulting heatmap closely mirrors the raw-basis result in Fig. 2: substantial layer- and module-wise misalignment persists, indicating preference-dependent sensitive directions that remain even with SVD basis.

F. Additional Results

F.1. Extended Analysis of Baseline Comparisons

In this section, we provide a more detailed analysis of the baseline comparisons presented in the main paper. We elaborate on the per-task performance metrics across both vision

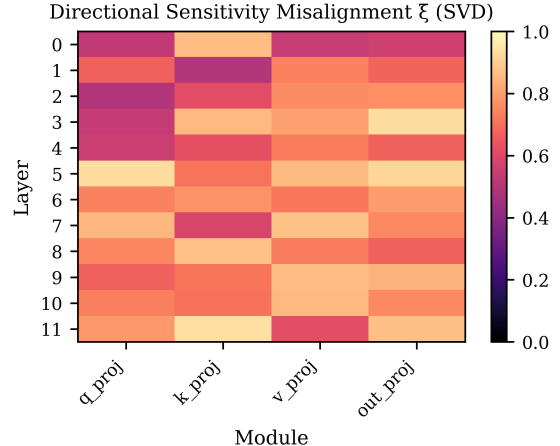


Figure 9. **Directional-sensitivity misalignment** $\xi(\rho_1, \rho_2)$ in the SVD basis.

and natural language inference (NLI) domains, offering an extended examination of the behavior of recent vanilla and LoRA-aware merging methods.

Per-Task Evaluation across Vision Tasks. For the eight image-classification benchmarks, Tab. 1 reports both the absolute per-task accuracies of the fine-tuned LoRA checkpoints and the normalized accuracies of the merged models. Strong vanilla merging methods such as Iso-CTS [60] reach up to 73.5% of the fine-tuned performance on average, but still lag behind the fine-tuned baselines and show large variance across datasets. Among LoRA-aware approaches, KnOTS-TIES [79] provides the strongest baseline, whereas RobustMerge [109] yields noticeably weaker average performance and smaller gains, indicating that its robustness benefits are limited in this setting. On top of these baselines, TARA-Variant A and TARA-Variant B further improve the average normalized accuracy to 74.0% and 76.3%, respectively, with consistent gains, showing that our method better preserves per-task performance when merging multiple checkpoints than more recent merging baselines.

Per-Task Evaluation on 6 NLI Tasks with LLMs. For the six NLI benchmarks, Tab. 2 shows a different picture from CLIP-based vision settings. Although Iso-C [60] performs strongly on vision benchmarks, in the NLI setting it produces highly unbalanced results: it attains more than 100% of the fine-tuned accuracy on SCITAIL, but suffers large drops on the other tasks, leading to the lowest average among recent vanilla baselines. EMR-Merging [31] and FR-Merging [115], which are effective in conventional CLIP-based multi-task setups, also fail to transfer cleanly to LLMs and do not achieve competitive averages in this regime. LoRA-aware methods generally improve over vanilla merging, but RobustMerge offers only modest gains over simpler LoRA-aware baselines, with limited improvement in average normalized accuracy. In contrast,

Table 5. To further address concerns regarding latency coming from gradient-based optimization, we experimented our method with LLaVA [50, 51] on merging six VQA experts.

Method	Dataset						Avg
	ScienceQA	VizWiz	IconQA	ImageNet	ChartQA	DocVQA	
<i>Per-task absolute accuracies (%)</i>							
Finetuned	86.6	69.7	65.2	96.0	39.3	41.2	66.4
<i>Per-task accuracies of merged models, normalized to finetuned (%)</i>							
TA [32]	81.6	71.3	57.2	43.6	66.6	79.5	66.6
TIES [99]	90.9	69.8	66.5	54.8	79.1	81.9	73.8
KnOTS-TIES [79]	87.4	77.0	60.5	44.8	76.5	85.6	72.0
AdaMerging [101]	87.9	81.0	66.3	47.0	74.5	76.1	72.1
TARA-Variant A	88.3	78.7	69.2	60.5	78.4	80.4	75.9
TARA-Variant B	89.1	79.2	69.5	59.6	78.3	80.0	76.0

Table 6. Time and memory cost analysis. We group baselines into gradient-free and gradient-based methods and compare their time and memory cost on LLaMA and LLaVA. For gradient-free methods, we exclude the time spent on grid search for tuning the scaling factor on the validation set. We report only *time per iteration* for gradient-free methods and all times measured in minutes (min). TIES, KnOTS-TIES, and TARA-Variant B require additional computation to resolve parameter conflicts or perform SVD, so we report both their total time and, in parentheses, the separate contributions from preprocessing and either one validation run (for gradient-free methods) or one optimization run (for gradient-based methods). Memory usage is reported as VRAM in MiB.

Method	LLaMA-3-8B		LLaVA-1.5-7B	
	Time (min)	VRAM (MiB)	Time (min)	VRAM (MiB)
TA [32]	3.6	16,150	10.6	14,814
TIES [99]	8.1 (4.5+3.6)	16,150	18.3 (7.7+10.6)	14,814
KnOTS-TIES [79]	10.8 (7.2+3.6)	16,150	24.3 (13.7+10.6)	14,814
AdaMerging [101]	8.0	19,918	13.9	19,788
TARA-Variant A	8.2	19,922	14.1	19,788
TARA-Variant B	15.2 (6.6+8.6)	20,040	27.7 (14.6+13.1)	20,662

our TARA-Variant A and TARA-Variant B reach 79.7% and 80.3% average normalized accuracy, respectively, outperforming all vanilla and LoRA-aware baselines. These results indicate that methods tailored to CLIP-based models do not automatically carry over to LLMs, while our approach scales robustly from vision to language tasks.

F.2. Evaluation on 6 VLM Tasks

We further evaluate the scalability of our method on vision–language models (VLMs). Specifically, we use LLaVA [50, 51] on six benchmarks: ScienceQA [57], VizWiz [25], IconQA [56], ImageNet [74], ChartQA [62], and DocVQA [64]. We fine-tune each LoRA adapter with rank 16 applied to the query, key, value and output projection modules of the attention layers, and train them for 500 iterations using AdamW [55] with a learning rate of 3×10^{-5} and batch size 1. We compare against vanilla model merging baselines, Task Arithmetic (TA) [32] and TIES [99], as well as the LoRA-aware methods KnOTS-TIES [79] and AdaMerging [101]. On LLaVA, AdaMerging underperforms LoRA-targeted merging methods such as KnOTS-TIES, indicating that its gains do not transfer well to the VLM regime. In contrast, both TARA-Variant A and TARA-Variant B achieve clear and stable improve-

ments over all baselines across the six benchmarks, confirming that our approach also works reliably in multimodal VLM scenarios.

F.3. Ablations and Time/Memory Analysis

Table 6 summarizes the empirical efficiency of each method in terms of time cost and peak VRAM. We apply rank-16 LoRA and merge six LLaMA and six LLaVA models on a single NVIDIA GeForce RTX 3090. The upper panel reports gradient-free methods, and the lower panel reports gradient-based methods. A key observation is that, even when merging six fine-tuned LoRA checkpoints at foundation-model scale, the peak memory usage only increases by about 4–5 GB, so gradient-based merging does not incur prohibitive VRAM overhead.

For time, we report the cost of a single validation evaluation for gradient-free methods and the total optimization time for gradient-based methods. At first glance, gradient-free and gradient-based approaches have similar per-run time, but gradient-free methods usually require multiple validation runs to tune the scaling factor λ , which substantially increases their effective cost. For example, tuning the Task Arithmetic scaling factor in $\mathbf{W}_{\text{merge}} = \mathbf{W}_0 + \lambda \sum_{i=1}^N \Delta \mathbf{W}_i$ with a grid from 0.3 to 0.7 in steps of 0.1 en-

tails five trials. If each evaluation takes 10.6 minutes, the total time rises to about 53 minutes.

Gradient-based methods do not require such grid search, so their total time can be more favorable. TARA has runtime comparable to AdaMerging but achieves higher accuracy. Methods such as TIES, KnOTS-TIES, and TARA-Variant B incur additional preprocessing to compute an SVD over all task vectors. For these methods, we therefore report both their total time and, in parentheses, a breakdown into preprocessing time and either one validation run for the gradient-free setting or one optimization run for the gradient-based setting. For six LLaMA-3-8B models, for instance, TARA-Variant B spends 6.6 of its 15.2 minutes on SVD preprocessing and the remaining 8.6 minutes on optimization, which is comparable to Variant A and AdaMerging. Even for large models such as LLaMA-3-8B and LLaVA-1.5-7B, a merge completes within 30 minutes, underscoring the practical applicability of TARA.

To complement the analysis on foundation models, we also evaluate computational efficiency on relatively lightweight vision targets. Table 7 reports the time and memory costs using the ViT-B/32 backbone. Consistent with the trends observed in larger models, the runtimes for learning-free methods (e.g., KnOTS-TIES, LoRA-LEGO) represent only a single validation pass. Because practical deployment requires grid searches to find optimal scaling factors, their total operational time typically exceeds the single-run optimization time of TARA. Regarding memory consumption, while a distinct gap in VRAM usage exists between learning-free and gradient-based methods on the smaller ViT-B/32 architecture, this discrepancy diminishes at the foundation-model scale (as seen with LLaMA-3). Since frozen base weights dominate the overall memory footprint of large models, the relative overhead introduced by gradient computation becomes less pronounced.

Table 7. Computational Cost (ViT-B/32). Times denote a single validation pass (learning-free) vs. optimization (learning-based).

Method	Time (min)	VRAM (MiB)
KnOTS-TIES [79]	2.8	2262
LoRA-LEGO [114]	4.0	1416
AdaMerging [101]	4.1	4344
TARA (Variant A)	4.1	4344
TARA (Variant B)	5.1	5922

F.4. Additional Ablation Studies

Ablation on Hyperparameter α . Figure 10 reports the effect of the STCH scaling hyperparameter α on normalized accuracy for both Variant A and Variant B. Performance is slightly degraded at very small scaling ($\alpha = 0.1$), but quickly stabilizes once α reaches 0.5. For $\alpha \geq 0.5$, both variants show only minor fluctuations and maintain consis-

tently strong performance across all benchmarks, indicating that our method is not sensitive to the exact choice of α in this range. Unless otherwise noted, we therefore fix $\alpha = 1$ in all main experiments.

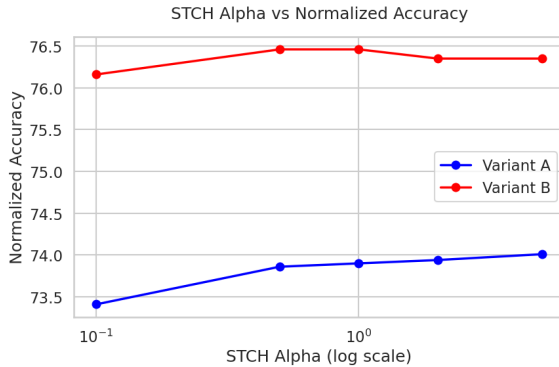


Figure 10. Ablation study of the hyperparameter α . Normalized accuracy is reported for two model variants across $\alpha \in \{0.1, 0.5, 1.0, 2.0, 5.0\}$. Both Variant A and Variant B exhibit stable performance over a wide range of α values, indicating that the method is not sensitive to this hyperparameter. Unless otherwise stated, we use $\alpha = 1$ for all main experiments.

Two-Task Pareto Fronts across Pairs. Figure 11 plots accuracy trade-offs for four task pairs on CLIP ViT-B/32. Sweeping the preference with TARA yields smooth Pareto fronts that are consistently dominant over AdaMerging, that is, TARA attains higher accuracy for the same preference across most of the preference range, especially in the balanced region where both tasks must be retained. Baseline mergers appear as isolated points and frequently lie below or off our front. We attribute this dominance to TARA’s LoRA-aware design: it preserves subspace coverage, retaining useful low-rank directions across tasks, while reweighting anisotropic directions to mitigate interference, keeping the merged model competitive near each task-optimal end without collapsing in the middle.

Robustness under Preference Perturbations. Figure 12 tests robustness with 8 tasks by fixing the two focal-task weights to 0.125 each (total 0.25) and randomly choosing the other six weights so they are nonnegative and sum to 0.75. Each scatter cloud shows 30 such samplings and the ellipses summarize their empirical covariance, with the mean marked by “ \times ”. Across all pairs, TARA produces tighter ellipses, indicating lower variance under preference perturbations, while AdaMerging shows larger spread. We also applied both a linear weighted-sum objective and a smooth Tchebycheff objective to TARA and to AdaMerging; the choice of objective yielded nearly identical ellipses and means.

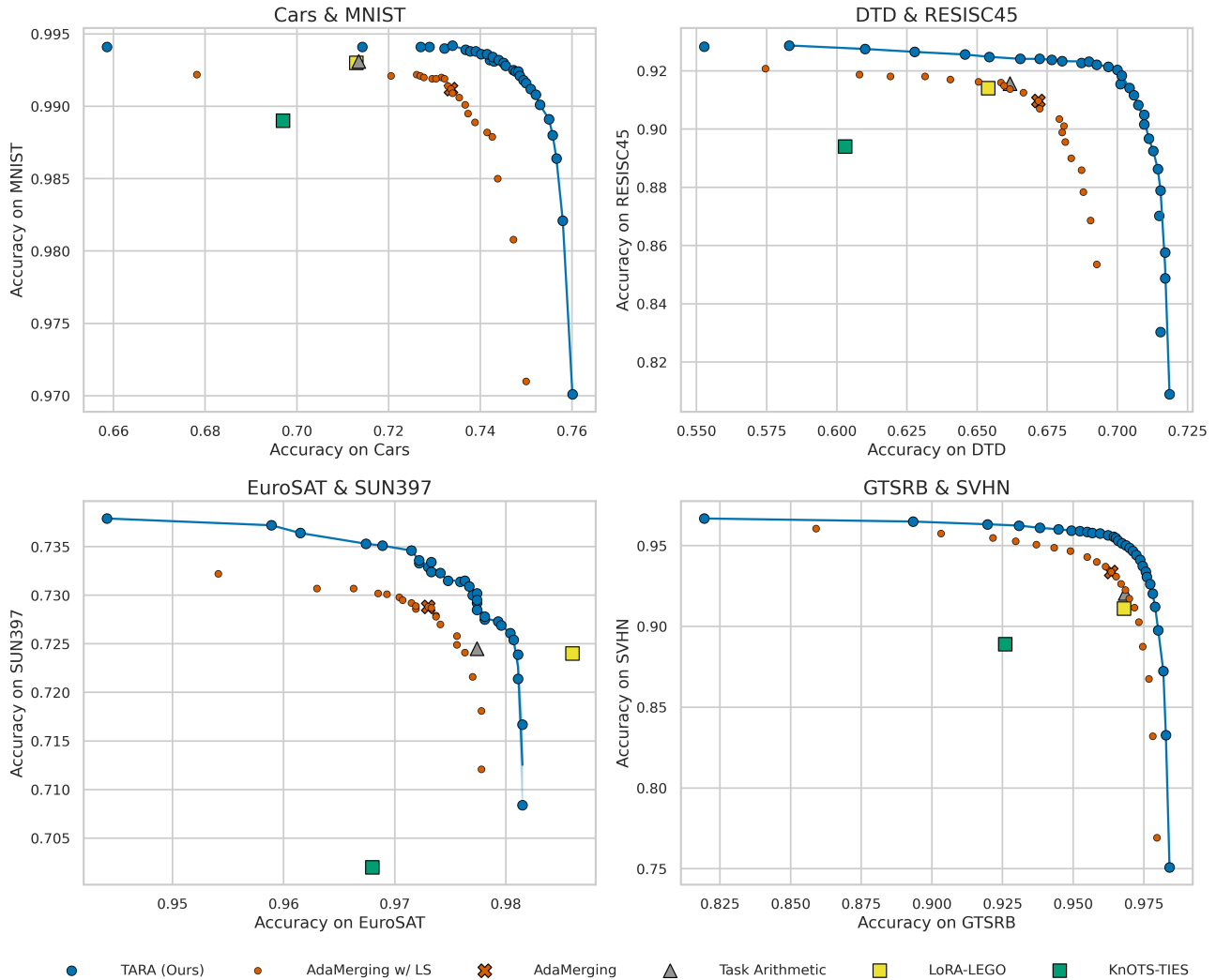


Figure 11. **Two-Task Trade-Offs on CLIP ViT-B/32.** Pairs shown from top-left to bottom-right: Cars-MNIST, DTD-RESISC45, EuroSAT-SUN397, GTSRB-SVHN.

Merging Models with LoRA Rank 16 on our Checkpoints. We complement the main-paper results (which use the KnOTS-released checkpoints [79]) with additional experiments on our own LoRA checkpoints to gauge robustness across sources. Specifically, we fine-tune CLIP ViT-B/32 adapters with a learning rate different from that used by KnOTS, and then evaluate the same merging protocols. Table 9 reports per-task absolute accuracies for the fine-tuned adapters (upper panel) and, for each merger, task-wise accuracies normalized to the corresponding fine-tuned baseline (lower panel). Table 11 reports generalization to unseen tasks on our checkpoints. The results are consistent with the main paper, indicating that the advantages of preserving subspace coverage and addressing anisotropy hold across different fine-tuning learning rates. A comparison of checkpoints is provided in Tab. 10.

Merging Models with LoRA Rank 4. LoRA is known to exhibit weaker cross-task alignment than full-rank fine-tuning, so LoRA-aware merging becomes especially important at low ranks. Using our CLIP ViT-B/32 checkpoints fine-tuned with rank-4 adapters, we evaluate vanilla and LoRA-aware merging in Table 12. Vanilla methods (e.g., TIES) degrade substantially, LoRA-aware baselines (KnOTS-TIES, LoRA-LEGO) recover more accuracy, and TARA achieves the strongest results overall: Variant B (500 iters) attains the best average normalized accuracy at **90.5%** and leads on most datasets. These rank-4 outcomes mirror the trends at higher ranks and underscore the benefit of modeling subspace coverage and anisotropy in low-rank LoRA merging.

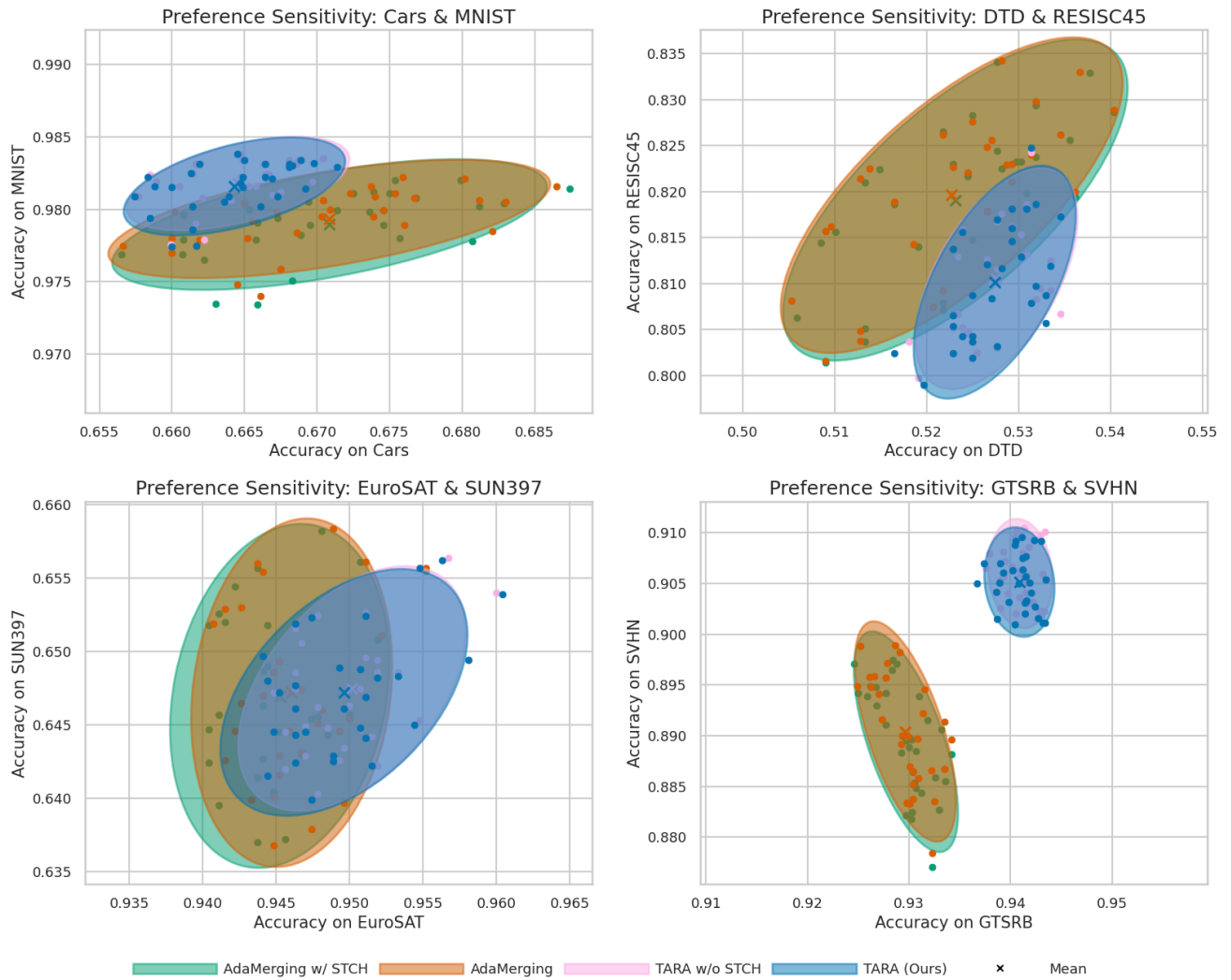


Figure 12. **Preference Sensitivity under Random Global Preferences.** Pairs shown from top-left to bottom-right: Cars-MNIST, DTD-RESISC45, EuroSAT-SUN397, GTSRB-SVHN.

Table 8. Eight CLIP/ViT-B-32 Models Joint-Task Results.

Method	Metric	Joint-Task Performances (%)								
		Cars	DTD	EuroSAT	GTSRB	MNIST	RESISC45	SUN397	SVHN	Avg
TA [32]	Hits@1	60.7	40.7	15.3	38.8	31.8	59.7	61.9	29.2	43.5
	Hits@3	84.9	63.7	23.0	66.1	48.4	83.6	83.9	50.1	65.2
	Hits@5	92.0	74.0	31.0	77.9	55.7	90.2	89.9	61.6	74.0
TIES [99]	Hits@1	60.4	39.7	13.0	35.0	33.4	58.6	61.3	32.9	43.6
	Hits@3	84.9	61.9	21.9	63.3	48.2	82.8	83.7	53.6	65.3
	Hits@5	92.1	72.4	29.0	75.3	54.0	89.4	89.9	64.1	73.9
DARE-TIES [107]	Hits@1	60.8	39.3	12.8	33.7	34.3	57.5	60.4	35.5	44.0
	Hits@3	85.3	61.4	18.1	63.6	50.2	82.3	82.6	57.8	66.4
	Hits@5	92.6	73.0	20.9	74.6	55.7	89.0	89.1	69.5	75.1
AdaMerging [101]	Hits@1	58.7	37.9	18.1	36.7	51.6	57.4	63.1	61.6	48.1
	Hits@3	83.1	59.5	56.9	63.6	71.0	81.3	84.8	85.1	73.2
	Hits@5	91.0	70.5	72.7	75.9	80.7	89.1	90.8	92.8	83.0
KnOTS-TIES [79]	Hits@1	61.7	40.5	16.2	44.2	39.1	59.0	60.6	36.7	46.8
	Hits@3	85.8	63.8	22.3	69.0	52.6	83.9	82.8	58.4	68.1
	Hits@5	92.6	74.5	31.1	79.8	58.4	90.4	89.1	68.5	76.3
KnOTS-DARE-TIES [79]	Hits@1	60.4	40.3	15.9	41.9	34.6	58.4	60.4	34.8	45.2
	Hits@3	85.0	63.5	21.1	68.4	50.0	83.8	82.4	56.5	66.9
	Hits@5	92.2	74.5	26.6	78.9	55.9	90.4	88.9	67.4	75.3
LoRA-LEGO [114]	Hits@1	60.3	39.9	15.9	41.6	29.8	57.6	60.1	30.2	43.1
	Hits@3	84.5	61.8	19.5	68.8	47.8	82.8	82.3	51.2	65.0
	Hits@5	91.8	74.0	21.1	78.3	56.9	89.7	88.8	63.5	73.9
TARA-Variant A	Hits@1	60.8	39.5	15.2	39.9	65.2	59.0	63.2	65.7	51.1
	Hits@3	84.8	60.8	58.0	67.0	80.7	82.6	85.2	87.8	75.9
	Hits@5	92.2	71.8	74.9	78.2	86.4	89.9	91.0	95.0	84.9
TARA-Variant B	Hits@1	63.2	40.1	12.1	41.9	64.6	62.1	63.6	46.4	49.3
	Hits@3	87.0	61.3	56.3	67.0	83.5	84.7	85.5	74.2	74.9
	Hits@5	93.4	72.5	76.9	77.2	88.9	90.9	91.3	89.9	85.1

Table 9. Using our checkpoints. Per-task accuracy on eight image-classification benchmarks. We merge eight ViT-B/32 checkpoints, each finetuned with LoRA. The upper panel shows the per-task absolute accuracy of the finetuned baselines; the lower panel reports accuracy of merged models, normalized by their corresponding finetuned baseline (%).

Method	Dataset								
	Cars	DTD	EuroSAT	GTSRB	MNIST	RESISC45	SUN397	SVHN	Avg
<i>Per-task absolute accuracies (%)</i>									
Finetuned	76.2	72.5	98.6	98.3	99.2	93.1	73.7	96.7	88.5
<i>Per-task accuracies of merged models, normalized to finetuned (%)</i>									
Vanilla Merging									
TA [32]	85.6	70.8	81.9	89.1	97.9	81.9	89.1	91.9	86.0
TIES [99]	72.2	61.2	64.7	66.6	90.0	70.0	86.1	73.7	73.1
DARE-TIES [107]	73.0	62.7	56.1	63.6	85.7	69.6	86.2	71.5	71.0
AdaMerging [101]	87.7	71.2	96.3	94.4	98.7	87.3	86.8	91.9	89.3
LoRA-aware Merging									
SVD [84]	76.0	60.9	74.8	90.4	98.1	74.2	85.0	93.6	81.6
Linear [59]	74.9	67.3	68.4	67.6	91.7	72.9	86.7	75.3	75.6
KnOTS-TIES [79]	85.4	69.3	77.8	76.6	93.3	80.1	89.4	82.0	81.7
KnOTS-DARE-TIES [79]	84.1	68.7	77.9	78.6	94.4	80.1	89.8	83.8	82.2
LoRA-LEGO [114]	84.9	71.4	82.7	91.1	98.5	81.2	87.4	93.4	86.3
TARA-Variant A	87.2	72.5	96.5	95.7	99.0	87.0	88.0	93.7	89.9
TARA-Variant B	85.8	72.0	96.8	96.4	99.1	88.0	87.4	95.2	90.1

Table 10. Comparison between merging methods between our checkpoints and KnOTS checkpoints.

Method	Dataset								
	Cars	DTD	EuroSAT	GTSRB	MNIST	RESISC45	SUN397	SVHN	Avg
<i>Per-task absolute accuracies (%)</i>									
Finetuned (KnOTS)	74.0	58.3	99.0	92.7	99.3	88.4	64.5	96.2	84.1
Finetuned (Ours)	76.2	72.5	98.6	98.3	99.2	93.1	73.7	96.7	88.5
<i>Per-task accuracies of merged models, normalized to finetuned (%)</i>									
TA [32] (KnOTS)	82.0	73.6	48.8	42.1	53.1	71.5	97.5	41.2	63.7
TA [32] (Ours)	83.1	68.7	79.7	93.0	98.8	79.4	85.2	93.8	85.2
TARA-Variant A (KnOTS)	84.5	76.2	68.9	39.4	82.2	72.8	97.5	70.0	73.9
TARA-Variant A (Ours)	86.5	72.0	94.4	95.0	98.8	85.3	87.4	93.5	89.1
TARA-Variant B (KnOTS)	86.2	78.4	76.8	42.9	82.7	75.4	98.6	69.7	76.3
TARA-Variant B (Ours)	86.1	72.7	95.7	95.6	99.0	86.4	88.0	94.2	89.7

Table 11. Using our checkpoints. Generalization results on two unseen tasks when merging ViT-B/32 models trained on six tasks.

Method	Seen Tasks							Unseen Tasks			All Tasks
	Cars	DTD	GTSRB	RESISC45	SUN397	SVHN	Avg Acc	EuroSAT	MNIST	Avg Acc	Avg Acc
<i>Per-task accuracies of merged models, normalized to finetuned (%)</i>											
TA [32]	85.6	73.0	94.7	82.4	88.4	95.0	86.5	47.3	78.1	62.7	80.6
TIES [99]	76.5	62.5	71.4	73.3	87.5	75.0	74.4	49.0	64.5	56.8	69.9
KnOTS-TIES [79]	85.0	69.4	83.9	81.1	89.4	84.8	82.3	56.6	73.4	65.0	78.0
KnOTS-DARE-TIES [79]	85.7	69.3	85.0	81.4	90.3	86.4	83.0	56.7	74.0	65.4	78.6
LoRA-LEGO [114]	85.2	72.9	94.9	82.3	88.3	94.8	86.4	46.9	77.8	62.4	80.4
AdaMerging [101]	87.1	73.8	93.4	91.2	88.4	96.2	88.4	52.2	83.1	67.7	83.2
TARA-Variant A	87.4	74.9	94.9	89.6	89.2	96.7	88.8	57.4	86.6	72.0	84.6
TARA-Variant B	87.2	74.7	95.4	89.4	89.3	96.7	88.8	63.4	87.7	75.5	85.5
<i>Per-task accuracies of merged models, normalized to finetuned (%)</i>											
TA [32]	87.2	75.6	86.4	95.6	98.4	90.6	89.0	60.4	61.6	61.0	82.0
TIES [99]	74.7	62.8	65.3	74.6	88.3	88.0	75.6	65.1	48.9	57.0	71.0
KnOTS-TIES [79]	86.7	70.8	80.8	83.3	94.1	90.4	84.3	67.5	57.2	62.4	78.8
KnOTS-DARE-TIES [79]	87.6	71.0	80.4	85.3	95.1	90.7	85.0	66.7	56.2	61.4	79.1
LoRA-LEGO [114]	87.0	75.3	86.0	95.9	98.5	90.2	88.8	60.0	61.5	60.8	81.8
AdaMerging [101]	89.7	74.7	96.7	95.0	99.4	90.4	91.0	60.1	63.7	61.9	83.7
TARA-Variant A	89.9	75.0	97.1	96.2	99.3	90.9	91.4	61.2	63.5	62.4	84.1
TARA-Variant B	89.7	74.9	97.4	96.4	99.2	91.0	91.4	60.7	58.6	59.7	83.5

Table 12. Using our checkpoints with LoRA (Rank-4). Per-task accuracy on eight image-classification benchmarks. We merge eight ViT-B/32 checkpoints, each finetuned with LoRA. The upper panel shows the per-task absolute accuracy of the finetuned baselines; the lower panel reports accuracy of merged models, normalized by their corresponding finetuned baseline (%).

Method	Dataset								
	Cars	DTD	EuroSAT	GTSRB	MNIST	RESISC45	SUN397	SVHN	Avg
<i>Per-task absolute accuracies (%)</i>									
Finetuned	72.1	70.2	98.4	98.1	99.2	93.3	73.4	96.7	87.7
<i>Per-task accuracies of merged models, normalized to finetuned (%)</i>									
Vanilla Merging									
TA [32]	87.4	76.2	74.0	78.1	98.1	83.7	89.7	92.3	84.9
TIE [99]	81.3	64.4	46.5	51.9	77.4	69.1	86.8	64.1	67.7
DARE-TIES [107]	81.2	65.4	50.9	48.4	76.3	69.8	86.7	63.5	67.8
AdaMerging [101]	87.9	75.1	94.7	92.0	98.2	86.9	89.5	91.1	89.4
LoRA-aware Merging									
SVD [84]	80.5	62.7	40.6	73.7	94.4	69.3	87.3	92.4	75.1
Linear [59]	44.0	25.6	12.4	37.8	71.5	23.3	44.2	51.7	38.8
KnOTS-TIES [79]	88.2	72.2	72.5	62.3	89.7	79.3	89.5	77.0	78.8
KnOTS-DARE-TIES [79]	87.7	73.0	73.4	65.0	90.4	79.9	89.5	78.8	79.7
LoRA-LEGO [114]	88.2	75.8	74.8	76.9	97.5	83.8	90.4	91.5	84.8
TARA-Variant A	88.7	76.4	94.9	92.1	98.3	86.8	90.0	92.0	89.9
TARA-Variant B	89.8	76.7	94.6	92.8	98.4	88.0	90.1	93.2	90.5

Ablation Study on LoRA Rank. We evaluate the impact of varying LoRA ranks r on the merging performance using the ViT-B/32 backbone. Table 13 presents the absolute and normalized accuracy across different rank configurations. TARA achieves higher accuracy than the baselines across all evaluated ranks. Notably, in the ‘Full’ setting, where the LoRA rank matches the ViT embedding dimension to emulate full-parameter fine-tuning, TARA does not simply converge to the FFT merging solution, rather, it maintains a distinct performance margin.

Table 13. Absolute (Normalized) Accuracy across LoRA Ranks.

Method	r=4	r=16	r=64	r=256	Full
TA [32]	71.9(82.9)	76.2(86.2)	77.9(86.2)	77.1(85.3)	72.0(80.8)
Adamerging [101]	76.3(87.2)	78.7(88.5)	80.2(88.7)	79.8(88.6)	79.1(88.2)
TARA	77.5(88.8)	80.5(90.6)	81.9(90.5)	80.9(89.7)	80.5(89.5)

Efficiency Analysis with Recent Baselines To assess computational efficiency, we compare TARA against recent gradient-based merging methods, CALM [100] and FW-Merging [5], using the CLIP-ViT-B/32 backbone. Table 14 reports the average accuracy, runtime, and peak memory (VRAM) usage. The results indicate that TARA requires significantly less runtime and memory overhead while maintaining competitive accuracy compared to other gradient-based approaches.

Table 14. Comparison with Recent Baselines.

Method	Adamerging [101]	CALM [100]	FW-Merging [5]	TARA-variant B
Avg. Acc.	78.7	80.0	77.9	80.5
Time (min)	4.1	20.0	13.4	5.1
VRAM (MiB)	4344	8066	7542	5922

Extended Evaluation on Vision Benchmarks. To verify the scalability of our approach, we extend the evaluation to different model scales (ViT-B/32 and ViT-L/14) and varying numbers of tasks (8, 14, and 20) following settings similar to those in FW-Merging [5]. As detailed in Tab. 15, TARA consistently demonstrates comparable or superior absolute and normalized accuracy across these configurations relative to recent baselines. This performance gap is particularly evident in large-scale settings, such as merging 20 tasks with the ViT-L/14 backbone.

Table 15. Absolute (Normalized) accuracy on vision benchmark.

Backbone (# Tasks)	TA [32]	AdaMer. [101]	CALM [100]	FW-Mer. [5]	TARA
ViT-B/32 (8)	76.2(86.2)	78.7(88.5)	80.0(90.6)	77.9(87.6)	80.5(90.6)
ViT-B/32 (14)	73.6(83.6)	75.0(84.8)	74.7(84.6)	75.4(85.2)	75.4(85.2)
ViT-B/32 (20)	64.6(72.7)	66.6(74.8)	66.9(75.2)	68.2(77.2)	68.7(77.2)
ViT-L/14 (8)	88.0(95.8)	88.9(96.7)	83.0(90.3)	87.0(94.7)	88.9(96.7)
ViT-L/14 (14)	85.0(92.7)	85.2(93.0)	80.5(87.7)	85.7(93.6)	85.9(93.7)
ViT-L/14 (20)	80.7(87.2)	81.3(87.8)	78.5(84.5)	77.4(84.1)	81.5(88.0)